PERSPECTIVE | JANUARY 22 2025

Progress in mid-infrared optoelectronics for high-speed free-space data throughput

Special Collection: Mid-IR Photonics

Frédéric Grillot ; Thomas Poletti ; Salvatore Pes

APL Photonics 10, 010905 (2025)
https://doi.org/10.1063/5.0230260

APL Photonics PERSPECTIVE pubs.aip.org/aip/app

Progress in mid-infrared optoelectronics for high-speed free-space data throughput

Cite as: APL Photon. 10, 010905 (2025); doi: 10.1063/5.0230260
Submitted: 23 July 2024 • Accepted: 30 October 2024 •
Published Online: 22 January 2025

View Online Export Citation CrossMark

Frédéric Grillot,[1,2,a)] Thomas Poletti,[1] and Salvatore Pes[3]

AFFILIATIONS

[1] LTCI, Télécom Paris, Institut Polytechnique de Paris, 91120 Palaiseau, France
[2] Center for High Technology Materials, University of New-Mexico, Albuquerque, New Mexico 87106, USA
[3] III-V Lab, a joint Thales, Nokia and CEA laboratory, 91767 Palaiseau, France

Note: This paper is part of the APL Photonics Special Topic on Mid-IR Photonics.
[a)] **Author to whom correspondence should be addressed:** grillot@telecom-paris.fr

ABSTRACT

Free-space laser communications offer a promising alternative for broadband data transmission in places where fiber optics are impractical. This technology, particularly effective at the 1.55 μm wavelength in the near infrared, also has potential applications in the medium-wave infrared (MWIR, 3–5 μm) and long-wave infrared (LWIR, 8–14 μm) ranges. MWIR and LWIR are superior for transmission through fog, clouds, and dust, with LWIR offering stealth advantages thanks to natural thermal radiation. In addition, mid-infrared wavelengths benefit from reduced atmospheric scattering and signal distortion, making them much more reliable for free-space optical communications. Quantum cascade devices such as lasers, modulators, and detectors operating in the MWIR and LWIR ranges are seen as high-potential candidates for data transmission under poor weather conditions or in degraded environments. This Perspective reviews advances in mid-infrared optoelectronics and their applications in high-speed data transmission and integrated photonic technologies, offering insights for researchers and engineers working in this field.

I. INTRODUCTION

Free Space Optical (FSO) communications refer to the transmission of information using an optical carrier propagating in air or vacuum without the use of physical media or guided wave structures. This technology represents an effective solution for the worldwide development of high-speed communication links at low cost and with reduced infrastructure. FSO links can transmit information wirelessly over distances ranging from a few hundred meters to tens of thousands of kilometers, covering terrestrial, Unmanned Aerial Vehicle (UAV), airborne, space, and inter-satellite applications.[1] Typically, an FSO system is made of different optoelectronic elements such as a modulated optical source, whose beam is shaped by adaptive optical systems to compensate for atmospheric turbulence. Various modulation techniques can be employed for data transmission, by encoding information in the amplitude, phase, or frequency of the transmitted optical signal. The signal then passes through the atmosphere before being collected by a detector on the receiver side and demodulated to recover the information. At present, FSO systems use visible and infrared wavelengths, enabling very high data rates thanks to the use of high-frequency optical carriers. The low beam divergence of laser-based communications, unattainable by their RF-based counterparts, makes the optical signal discrete and difficult to detect, while improving energy efficiency. Moreover, these systems can be deployed quickly and cost-effectively even in complex environments, thanks to mobile ground stations.

To ensure seamless communication under challenging conditions, a hybrid system combining FSO and RF technologies is also a promising approach. In cases where communication is interrupted due to obstacles, or disruptive weather conditions, the system seamlessly switches to RF transmission, thus ensuring uninterrupted connectivity. Generally, RF communications are less sensitive to atmospheric conditions than those established at the standard telecommunication wavelength range around 1.55 μm, but they can still be disrupted by phenomena such as incoherent attenuation caused by rain. Under certain conditions, the FSO system can thus serve as the primary communication method, while the RF system acts as a relay network in case of disruption or adverse weather affecting the performance of the primary network. This hybrid configuration can find applications in various fields, including military communications, cellular networks, and high-speed Internet access in urban areas. Its ability to provide broadband communications and its adaptability to different environmental conditions make it a preferred choice in scenarios where reliability and continuous connectivity are paramount. An alternative approach, in which data are transmitted in two streams, can be envisaged: first, an FSO link, and then, to overcome the limitations, such as the need for line-of-sight communication, RF transmission is used for the last segment of the communication to transmit the data to the end user.

Traditionally, the selection of appropriate wavelengths for FSO systems has been based on atmospheric transparency windows, which are the regions of minimal atmospheric absorption (Fig. 1). These low-absorption windows are determined by the molecular composition of the air. Photon absorption by atmospheric molecules causes electronic transitions to higher vibrational or rotational energy levels, with the specific transitions depending on the molecule. As shown in Fig. 1, there are several weak absorption bands in the infrared spectrum, in particular, the short-wavelength infrared (SWIR) around 1–2.5 μm, the medium-wavelength infrared (MWIR) window between 3 and 5 μm, and the long-wavelength infrared (LWIR) window between 8 and 14 μm.[2] One of the main challenges facing FSO systems is their ability to withstand very hazy conditions, which result from the accumulation of water droplets in the atmosphere. This phenomenon leads to considerable scattering and attenuation, which particularly affects FSO systems. Not only absorption but also signal distortion is lower at higher wavelengths. Indeed, turbulence on the propagation path is known to considerably deteriorate the optical signal, causing, for example, beam broadening, beam wandering, scintillation, or loss of spatial coherence. In this case, scintillation will be the predominant phenomenon, corresponding to fluctuations in the intensity of the propagating beam. This effect evolves as a function of $\lambda^{-7/6}$, with λ being the operating wavelength, and will therefore be less important at longer wavelengths. The publication[1] provides information on beam attenuation values around 0.850 and 1.55 μm, as well as visibility values. To provide a more complete overview, Table I displays the beam attenuation due to Mie scattering in the SWIR, MWIR, and LWIR regions considering different visibility factors.

TABLE I. Beam attenuation in dB/km due to Mie scattering.[1]

	Attenuation (dB/km)		
Visibility (km)	$\lambda = 1.55\ \mu$m	$\lambda = 4\ \mu$m	$\lambda = 9\ \mu$m
20 (clear)	0.2	6×10^{-2}	2×10^{-2}
5 (haze)	1.2	0.47	0.2
2 (mist)	4	2	1.1
1 (fog)	9.3	5.4	3.3

So far, laser diodes operating in the SWIR have proven to offer the highest data rates and ranges for FSO links due to the small absorption coefficient through the atmosphere and the availability of reliable sources and detectors, with low power consumption and interesting modulation bandwidth. To increase the data rates significantly, multiplexed links can be used. Very recently, a 1.55-μm free-space link at a record data rate of 0.94 Tbit/s over a distance of 53 km and an elevation difference of 2800 m has been achieved.[3] This remarkable demonstration, which shows the potential of FSO technology, was realized through the use of optical amplification, polarization-division multiplexing, coherent detection, full adaptive optics, and error correction techniques. Several commercial FSO systems are already available,[4] such as MRV Connections, which has demonstrated a 10 Gbit/s link over 350 m or Nexus-10G$^{\rm TM}$, which is a fully reinforced, two-way solution for point-to-point terrestrial communications.[4,5] The latter boasts impressive data rates of up to 10 Gbit/s and can establish FSO links over distances of up to 5 km.

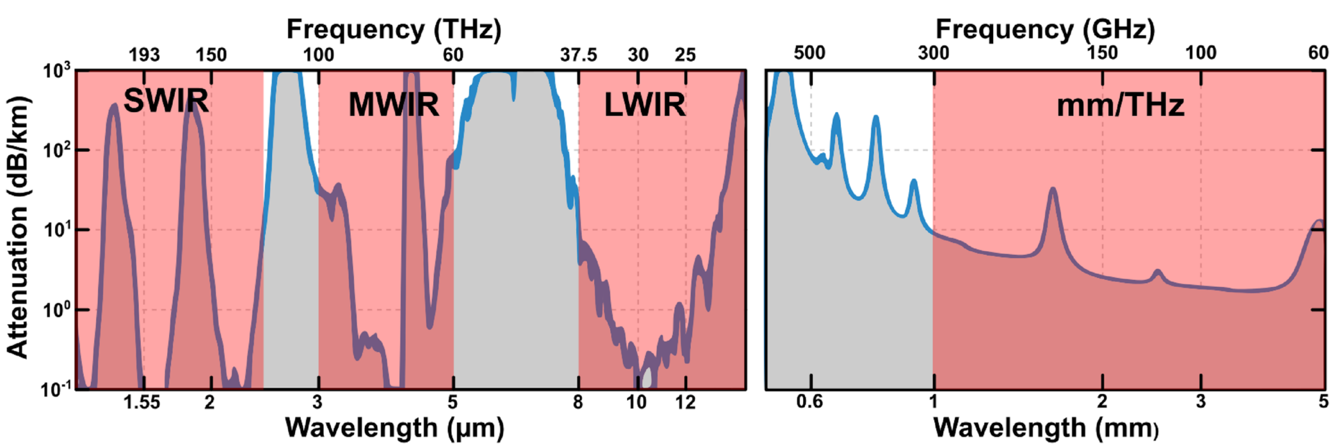

FIG. 1. Transmission through the atmosphere as a function of wavelength, calculated for a horizontal propagation at the ground level and a humidity of 50% (source: HITRAN[2]). The different transmission windows are indicated. From left to right: SWIR (1–2.5 μm), MWIR (3–5 μm), LWIR (8–14 μm), and part of the RF window (here covering the IEEE V, W, and G bands).

In addition, let us stress that the German Aerospace Center (DLR) has achieved a 1.72 Tbit/s link over 10.45 km. The current record for data rates was set on a laboratory bench by the DLR around 1 Pbit/s using OFDM-8QAM signals multiplexed at about 54 Gbit/s.[6] However, these systems all face reliability issues when exposed to severe atmospheric conditions such as clouds and fog, meaning that the link data rate can drop very quickly to very low levels. To overcome these limitations, in recent years, researchers have increasingly focused on mid-infrared sources due to their advantages in terms of resilience against degraded atmospheric conditions. In addition, as conventional channels for high-speed communications using near-infrared fiber are becoming increasingly solicited, it is of paramount importance to extend the current knowledge about near-infrared optics to the mid-infrared domain and to assess the performances of long-haul free-space transmissions. In addition, effective communication systems must also utilize advanced modulators, amplifiers, and detectors.

This Perspective therefore reviews the most promising achievements in mid-infrared optoelectronics (lasers, modulators, and detectors), as well as recent demonstrations of high-speed data throughput made possible thanks to mid-infrared technology. In Secs. II–IV, we, respectively, present the main active component developments for free space optical communications at mid-infrared wavelengths, laser sources, external modulators, and detectors. In Sec. V, we review the recent demonstrations and associated trends in FSO communications at mid- and long wave infrared wavelengths. We also provide some topical perspectives to this work in Sec. VI, including, but not limited to, the development of integrated photonic technologies, coherent communications, and FSO-to-RF transmission systems. We believe that this article can be useful to all researchers and engineers developing new solutions for optical data transfer in the MWIR and LWIR regions, which are envisioned to be promising for the future of communications, even though the current performances of mid-infrared components are still well behind those of their near-infrared counterparts.

II. LASER SOURCES

A. Quantum cascade lasers

The Quantum Cascade Laser (QCL) is a unipolar semiconductor laser, which differs fundamentally from the interband diode laser. Unlike the bipolar operation of the diode laser, where photon emission results from the recombination of electrons and holes between the valence and conduction bands [Fig. 2(a)], the QCL operates through radiative electronic transitions within the conduction band of semiconductor heterostructures [Fig. 2(b)], which further guide the electron flow by tunneling and scattering to establish electronic inversion for a pair of quantum levels at a given electric field.[7] In order to increase the total gain, a structure composed of several periods is typically used [Fig. 2(b] so that the electrons flow across the total structure like water in a cascade. The performance of QCLs deeply relies on complex quantum engineering, necessitating precise control of the growth of the superlattice structure to create quantum wells (QWs) and barriers with thicknesses on the order of a few nanometers that meticulously drive the electron movement and energy states, enabling the specific intersubband transitions required for laser emission.[8] The lasing emission range of QCLs typically extends from 3 to 300 μm, making them

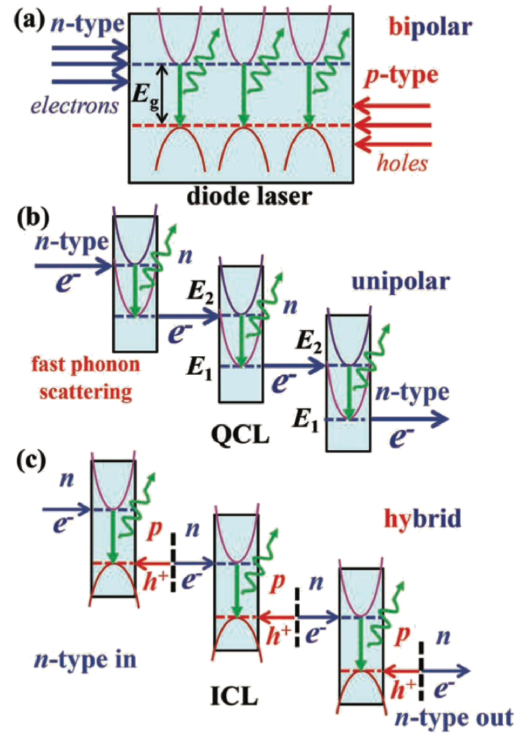

FIG. 2. (a) Conventional bipolar (electron and hole) diode laser. (b) Unipolar intersubband quantum cascade laser (QCL). (c) Interband cascade laser (ICL) combining the advantages of the first two. Reproduced with permission from R. Yang, Compd. Semicond. **25**, 48–53 (2019). Copyright 2019 Angel Business Comms. Ltd.[22]

candidates of choice for a wide range of applications such as spectroscopy, free-space laser communications, or Light Detection and Ranging (LIDAR). Thanks to considerable advances in molecular beam epitaxy (MBE) and bandgap engineering, the first functional QCL was achieved in 1994 at 4.2 μm in pulsed and cryogenic operation with a peak power in excess of 8 mW.[7] Further developments permitted the growth of QCL structures via metalorganic vapor phase epitaxy (MOVPE).[9] Other studies have focused on enhancing the QCL performance for room-temperature operation, higher output power, broader wavelength range, and single-frequency operation. However, it is known that QCLs face significant challenges such as phonon scattering loss, high heat generation, and structural losses. To address these issues, it is known that materials with higher thermal conductivity are required to improve heat dissipation.[10] In addition, refining the doping profile across the structure is required for enhancing carrier transport and reducing carrier leakage, leading to more compact and efficient devices that are desirable for practical applications. The first demonstration of a room-temperature QCL was reported in 1996 in pulsed operation.[11] Subsequent advances then led to the successful implementation of continuous-wave (CW) operation.[12,13] These groundbreaking achievements underscored the rapid progress in the field of QCLs and reinforced their potential as viable light sources for the aforementioned applications. These past years, QCLs have gathered even more attention because of their ability to generate broadband frequency combs.[14] Frequency combs are coherent dynamic states emitted by a light source, which consist of a series of evenly spaced spectral lines in the frequency domain, distinguished by low amplitude and phase noise. The ultrafast gain dynamics and broad gain spectrum of QCLs make them efficient for broad comb generation, which is highly useful for dual-comb spectroscopy[15,16] and LIDAR technology.[17] Moreover, it was also shown that a customized ring QCL with an egg-shaped cavity can produce a quantum walk in synthetic frequency space [Fig. 3(a)].[18] Indeed, the fast gain modulation enables coupling between the comb frequency lines through interferences in the ring laser, hence resulting in a quantum-mechanical random walk with a broad and uniform distribution of light intensity at different frequencies [Fig. 3(b)]. Developing high power QCLs is also crucial for FSO applications. Achieving high power operation requires optimizing the Wall-Plug-Efficiency (WPE). Increasing the number of stages, improving the confinement factor, reducing the waveguide loss, and decreasing the current threshold are some directions to be considered in order to maximize the output power. However, increasing the number of QWs should be done carefully, otherwise it would degrade the performance, leading to a higher device resistance and thermal effects. Improvements in heat dissipation have resulted in the demonstration of a 27% WPE at room temperature in pulsed mode operation, achieving a maximum power of 12 W at 4.9 μm.[19] Other recent results reported QCLs reaching 14 W in pulsed operation at room temperature[20] and 5 W output power in CW operation at room temperature.[21]

Distributed feedback (DFB) lasers are essential components in optical communications due to their ability to provide stable, single-wavelength operation with narrow line. The first demonstration of a DFB operation was made only 4 years after the initial demonstration of QCL.[24] The idea of DFB is to be able to select one lasing wavelength within the cavity. In a wide range of applications, including multi-wavelength communication systems and spectroscopy,[25,26] the use of a single frequency laser is crucial for several reasons. Indeed, DFB lasers offer valuable advantages in precise spectroscopic systems due to their high stability and exceptional spectral purity. Their single-frequency operation is particularly beneficial for implementing multi-wavelength channel links without encountering interference issues. Furthermore, the requirement of single mode operation is also important for various components such as external modulators as it guarantees their optimal performance. The various developments in nano-fabrication have enabled the development of high-quality gratings, resulting in reliable DFB QCLs.[23] For example, Lu *et al.* demonstrated impressive high-power single-mode operation of 2.4 W at 4.8 μm [Fig. 3(c)].[23] Furthermore, DFBs have been developed in the 7.2 μm range with an impressive output power as high as 550 mW.[27] Long-wavelength (>17 μm) CW and room-temperature DFB QCLs have also been demonstrated, providing a high output power.[28] However, for high speed modulation purposes, processing short ridges in DFB QCLs is still challenging as the optical gain significantly reduces and cannot compensate for ridge losses below 1 mm, hindering room-temperature operation. However, the implementation of high-efficiency external modulator systems greatly benefits from the use of high-power CW DFB lasers. Last but not least, it is relevant to note that recent studies about lab-on-a-chip mid-infrared spectroscopy are already weighing in photonics integrated circuits (PICs) at mid-infrared wavelengths.[29]

Finally, the terahertz (THz) domain, which is the frequency region between infrared and microwaves, spans from 0.1 to 10 THz,

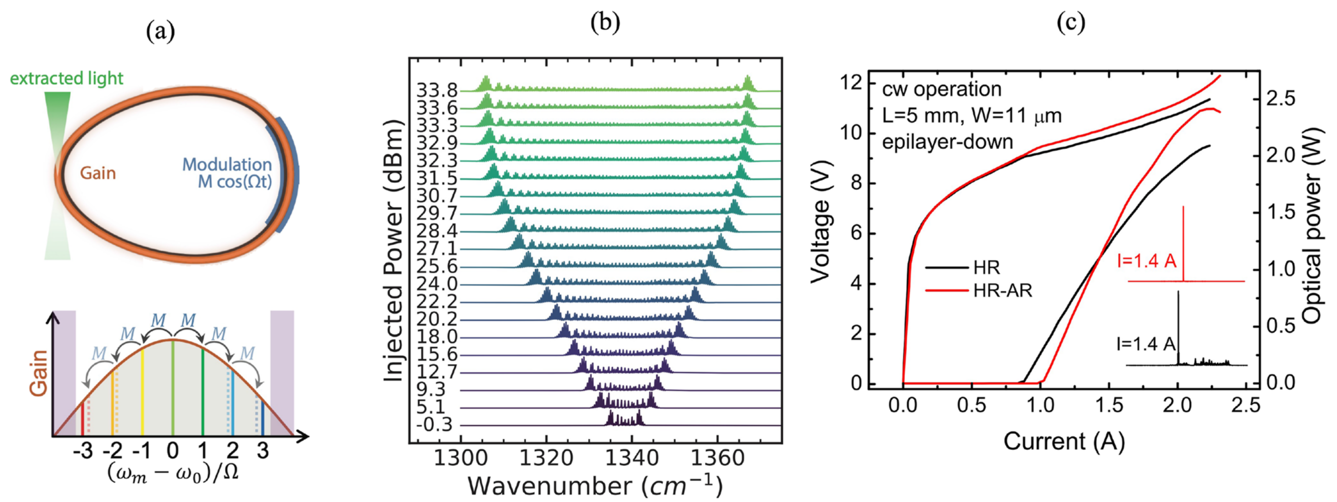

FIG. 3. (a) The optical modes in a deformed circular cavity are coupled via resonant modulation, inducing nearest-neighbor gain and the proliferation of a synthetic photonic lattice in frequency space, whose bandwidth is fundamentally limited by the dispersion (indigo). In analogy to the quantum harmonic oscillator, the zeroth order supermode corresponds to a Gaussian pulse (red) in the discretized frequency. (b) Quantum walk comb device measured under RF injection. The progressive broadening of the quantum walk spectra is observed with increasing injection power. (a, b) Reproduced with permission from Heckelmann *et al.*, Science **382**, 434–438 (2023). Copyright 2023 AAAS.[18] (c) CW PIV characteristic of a DFB-QCL at room temperature. The ridge width and cavity length of the QCL-DFB device are 11 μm and 5 mm, respectively. The rear facet is HR coated, and the device is epilayer-down bonded to a diamond submount. The inset shows the optical spectra before AR coating (lower inset) and after AR coating (upper inset). Reproduced with permission from Lu *et al.*, Appl. Phys. Lett. **98**, 181106 (2011). Copyright 2011 AIP Publishing.[23]

and during the past two decades, intersubband technology strongly contributed to the development of THz emitters and receivers. Terahertz QCLs were first demonstrated in 2001[30,31] under pulsed operation in a liquid-helium flow cryostat environment and then extended to CW operation above liquid-nitrogen temperature,[32] and the latest efforts are paving the way for THz QCLs without the need for cryogenic cooling.[33,34] Alternatives were also proposed to increase the maximum temperature of operation of THz QCLs, such as the application of a strong magnetic field above 16 T, in order to suppress the inter-Landau-level non-radiative scattering.[35] Another scheme, avoiding thermal relaxation mechanisms between upper and lower laser levels through optical phonons that are currently detrimental to room-temperature intersubband THz QCLs, is based on difference frequency generation (DFG) in a mid-infrared QCL. This has led to THz room-temperature sources with an output peak power up to a few mW.[36]

B. Interband cascade lasers

The interband cascade lasers (ICLs) combine the peculiar advantages of QCLs and conventional bipolar diode lasers. It exploits radiative transitions between the conduction band and the valence band [Fig. 2(c)]. The structure of an ICL is very similar to that of a QCL, in that it is based on a cascade design of heterostructure bands.[37] This design preserves the advantages of cascade injection and the flexibility to tailor the emission wavelength through band-structure engineering.[38] However, due to the nature of interband transitions, electrons and holes pass through the heterostructure, meaning that carrier dynamics is much slower than that in QCLs. This also leads to the birth of relaxation oscillations close to the gigahertz, which is a good prerequisite for achieving high-speed data transfer using direct modulation of light.[39] From a general viewpoint, ICLs can operate in the mid-infrared at room temperature and with low power consumption, which is an additional advantage for energy-efficient optical communications. In space industry, ICLs were used in the methane detector aboard the NASA Curiosity rover.[40] The first experimental demonstration of ICLs was carried out on a structure composed of 20 active stages and featured a high threshold current density in pulsed operation at temperatures ranging from 80 to 120 K.[41] Over the years, significant improvements have been made by introducing multiple QW configurations into the ICL design.

Although ICLs initially only worked in pulsed mode operation at temperatures below 200 K,[42–45] a major breakthrough came up with the demonstration of pulsed mode operation at room temperature.[46] The development of CW operation was then accelerated by using the W-shaped QW design, which significantly increased the electron–hole recombination and lowered the current threshold. The first demonstration of a CW ICL was carried out in 2008.[47] This achievement was made possible by a number of modifications to the device. First, the number of stages was reduced to 5 to minimize the threshold current. Second, separate n-doped GaSb confinement layers were introduced on either side of the active core. Third, the doping concentration and thickness of the confinement layer were optimized to reduce heat generation. These developments have resulted in the creation of highly efficient devices that can achieve an output power of 300 mW for the Fabry–Pérot cavity or 50 mW for the DFB in CW operation. These devices operated at room temperature and emitted in the 3–5 μm wavelength range.[48] A year later, the same group reported nearly 600 mW CW output power of a seven-stage narrow ridge Fabry–Pérot ICL with corrugated sidewalls and thicker separate confinement layers.[49] ICLs are particularly interesting for integration on silicon because of their low-power consumption.[48,50] Furthermore, they have proven to be relatively resistant to defects (a direct consequence of the type II QW structure), such as threading dislocations.[51,52] As shown in Fig. 4, ICLs directly grown on silicon can exhibit performances similar to their counterparts grown on native GaSb with output powers beyond 10 mW at room temperature.[53] The capability to manufacture high-quality mid-infrared lasers integrated on silicon constitutes a huge potential of this technology,[54] as this means capability for large-scale production on the one hand[55] and compact versatile systems on a chip on the other hand.

Furthermore, there have been recent efforts to extend the lasing operation to the LWIR range, but this faces several challenges. First, the InAs/AlSb superlattice utilized for the optical cladding layers needs to be significantly thicker to accommodate the longer decay length of the optical wave, which complicates the growth process using MBE. Second, the superlattice exhibits low thermal conductivity, so increasing its overall thickness would also raise the thermal resistance of the device, thereby impacting its performance. Finally, the reduced optical confinement as well as the rise of free carrier absorption (which roughly scales quadratically with wavelength) results in a rapid increase in the laser waveguide losses. This last point is generally true for active components as ICLs[56] and QCLs,[57] as well as for passive optical waveguides, and depends on the doping of the waveguides' cladding layers, which are intended to provide carriers to achieve population inversion in the active region of the lasers. Despite that, it is important to highlight two recent results. One showed continuously lasing ICL at 11 μm at cryogenic temperatures with an output power of 14 mW.[58] The other reported the longest CW wavelength near 13.2 μm in the LWIR region from an ICL having a QW active region made with strained layers.[59]

As already mentioned, single mode lasers are of paramount importance in spectroscopy and high-speed communication systems. Laterally coupled gratings developed by Nanoplus can be employed for achieving DFB ICLs emitting between 2.7 and 7 μm. To this end, a 2.4 mm long and 9.8 μm wide ridge device with as-cleaved facets achieved single mode CW operation with an output power around 10 mW at 25 °C at 3.4 μm.[60] Thorlabs also demonstrated longitudinally segmented DFB gratings with 42 mW at 3.3 μm at 25 °C for ridges with widths of 10 μm.[61] Other configurations like those developed by the Naval Research Laboratory involved corrugated waveguides to increase the output power by broadening the ridge. Their single-mode DFB ICL emitted 55 mW in CW at 3.7 μm and at 25 °C.[48] They have also demonstrated DFB ICLs with Ge top cladding gratings operating in CW up to 80 °C. At 40 °C, for ridge widths of 7.4 μm and cavity lengths of 2 mm, a device output over 27 mW was reported with a side-mode suppression ratio (SMSR) over 30 dB.[62] Meanwhile, we can also mention the realization of single mode ICLs using slotted waveguides, where the main difference with DFB technology is that the periodic spacing is much greater than the wavelength. Here, the main advantage is that standard UV photolithography can be used. A recent development showed slotted ICLs emitting from a single longitudinal mode at 3.5 μm and 2 mW of output power per facet at 20 °C with threshold

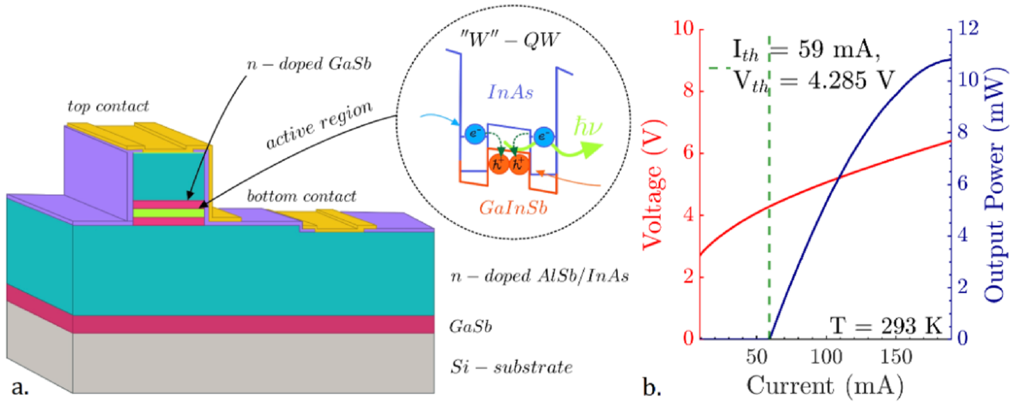

FIG. 4. (a) Schematic representation of the ICL directly grown on Si. (b) Light-intensity–voltage characteristics of the 3.5-μm epitaxial ICL on silicon. Reproduced with permission from Zaminga *et al.*, *2023 IEEE Photonics Conference (IPC)*. Copyright 2023 IEEE.

currents around 80 mA.[63] Vernier tuning using multisection devices whose emission profile depends on the interference of two single-mode waveguides can also be considered. For instance, combining two DFB-ICL sections, a discontinuous tuning of 158 nm was achieved at room temperature in CW mode along with an output power of 3.5 mW at 3.7 μm.[64] Another approach for making a widely tunable single mode laser is to directly couple light from the laser into an external cavity formed by the collimation lens/mirror and a diffraction grating in a Littrow configuration. Then, the wavelength selection is performed by rotating the external grating element to select a different resonant cavity mode.[65] By using a V-coupled cavity, ICLs capable of single-mode emission with a tuning range exceeding 100 nm near 3.4 μm were demonstrated.[66]

C. Which laser for FSO applications?

For applications in FSO communications, multiple requirements are important to consider to best choice which type of laser to use. The first one is obviously the wavelength of operation. If a wavelength in the LWIR (8–12 μm and more) is required, there is no other alternative than QCLs, which are the only technologically mature laser addressing this band. Meanwhile, when it comes to MWIR wavelengths, both QCLs and ICLs can be employed, and the choice has to be driven by other metrics specific to the foreseen application. Energy consumption, optical output power, electro-optical bandwidth, and spectral purity are the main metrics to be considered in that case. In general, a QCL consumes a lot of electrical power but also emits a higher optical power than an ICL. Interestingly, both ICLs and QCL have nevertheless comparable wall plug efficiencies,[67,68] but the latter necessitates a good active thermal dissipation to work properly, which can be both cumbersome and energy consuming. In applications where compactness and energy efficiency are of primary importance, ICL might be a better option, provided that the requirement on the output optical power is met, and then comes the electro-optical bandwidth of the source. This is primarily important for applications requiring direct modulation of the laser. In this domain, there is a big difference between ICLs and QCLs, as stated in Secs. II A and II B. Indeed, ICLs are bipolar devices; both electrons and holes participate to transport through the semiconductor heterostructure. Conversely, QCLs are unipolar devices, where electrons are the only carriers involved, benefitting from very fast transport mechanisms such as phonon assisted tunneling. Therefore, the intrinsic bandwidth of QCLs lies in the hundreds of GHz, while it is at least an order of magnitude lower in ICLs.[69,70] When fast direct modulation is required, QCLs should thus be preferred. In conclusion, at present, QCLs are the main (if not the only) option for addressing the LWIR window, for applications requiring a high output power with a relaxed constraint on the energy consumption, and when very fast direct modulation is required. Meanwhile, at MWIR wavelengths, ICLs offer a better performance in terms of energy consumption, whenever a very fast (tens of GHz) modulation is not of uttermost importance and neither is a high output power (several tens of mW).

III. MODULATORS

Modulators are one of the main components of photonic circuits. At mid-infrared wavelengths, despite its interest, the development of such a fundamental building block is nevertheless still lagging behind that of other active components such as lasers or detectors. Several physical mechanisms can be employed to produce an electro-optical modulation, which are mostly directly inspired to what works best at traditional telecommunication wavelengths.

A. Free carrier plasma dispersion effect

The free carrier plasma dispersion (FCPD) effect results from the interaction between free carriers and the optical electric field. By tuning the local free carrier density in a material, in most cases with an applied external electric field, one can change its local optical dielectric constant. This effect can be modeled by a Drude contribution to the dielectric constant, which affects both the real and imaginary parts of the material's optical index. Advantageously, the modulation strength of both the optical index and material absorption, for a given free carrier density, tends to increase with the optical wavelength and scales as λ^p, where p ranges between 2 and 3.[71] This characteristic makes the FCPD particularly interesting for mid-infrared photonics and also a wideband effect.

Modulators based on the plasma dispersion effect have been using either carrier injection or depletion in PN or PIN junctions[72–74] or similar structures, carrier accumulation in capacitive junctions, or even optical pumping in optical waveguides.[75] Their use in mid-infrared modulators has first been extensively studied for silicon-on-insulator (SOI) devices at classical telecommunication wavelengths, before being extended to the 2 μm band in the past decade. This band is indeed seen as a good candidate to address the future demand in data rates through the fiber network, using hollow-core photonic bandgap fibers compatible with 1550 nm technologies. The first reports of external modulators addressing that band are from 2012 by Van Camp *et al.*[72] who demonstrated a silicon-based Mach–Zehnder modulator (MZM) using carrier injection in a PIN junction. It showed a −3 dB bandwidth of 400 MHz (and up to 1.8 GHz with pre-emphasis), an extinction ratio (ER) as high as 23 dB for a $V_\pi L_\pi$ product of 0.012 V cm, and was used to demonstrate transmission up to 3 Gb/s. A few years later, such devices reached comparable performances to state of the art MZM modulators at 1550 nm using carrier depletion in a PN junction. Up to 20 Gb/s transmission rate was reported by Cao *et al.* using a MZM modulator at 2 μm, having a $V_\pi L_\pi$ of 2.68 V cm and an insertion loss of 13 dB,[76] and up to 80 Gb/s PAM-4 was demonstrated with a similar device by Wang *et al.*[77] In parallel, germanium-on-insulator (GeOI) devices have been explored, but their performances were limited by high absorption in the oxide layer.[78]

It is not until very recently that devices for the upper bound of the mid-infrared window have been investigated, pushed by the growing interest for free-space optical communications at those wavelengths. Since silicon itself becomes absorbent above 2.6 μm, this has been accompanied by a switch to the silicon–germanium (SiGe) and germanium (Ge) platforms to benefit from their reduced absorption at mid- and long wave infrared wavelengths, compatibility with mature CMOS process, and already developed passive photonic building blocks.[54,79,80] Carrier injection in PIN junctions was first reported in SOI and Ge on silicon modulators, both working as electro-absorption modulators (EAMs) and MZM at a wavelength of 3.8 μm, and also 8 μm for the Ge on silicon, but with limited 3 dB bandwidth not exceeding 60 MHz.[74,81] Meanwhile, EAM devices based on carrier depletion of a Schottky contact in graded index SiGe have reached a higher bandwidth, up to 1 GHz, with a limited extinction ratio not exceeding 1.3 dB for a 500 μm long waveguide.[82,83] More recently, employing a PIN junction in carrier injection mode embedded in SiGe waveguides, a higher extinction ratio could be reached, but with a much longer waveguide of 5.9 mm. ERs ranging from around 4 to 9.3 dB for wavelengths ranging from 6.4 to 10 μm have been reported, and an electro-optical bandwidth limited to 200 MHz.[84] The latter device geometry and measured performance are reproduced in Figs. 5(a) and 5(b). The insertion losses of the devices were also limited, from 1.4 to 9.3 dB from 6.4 to 10 μm respectively. Interestingly, no other type of FCPD based modulator

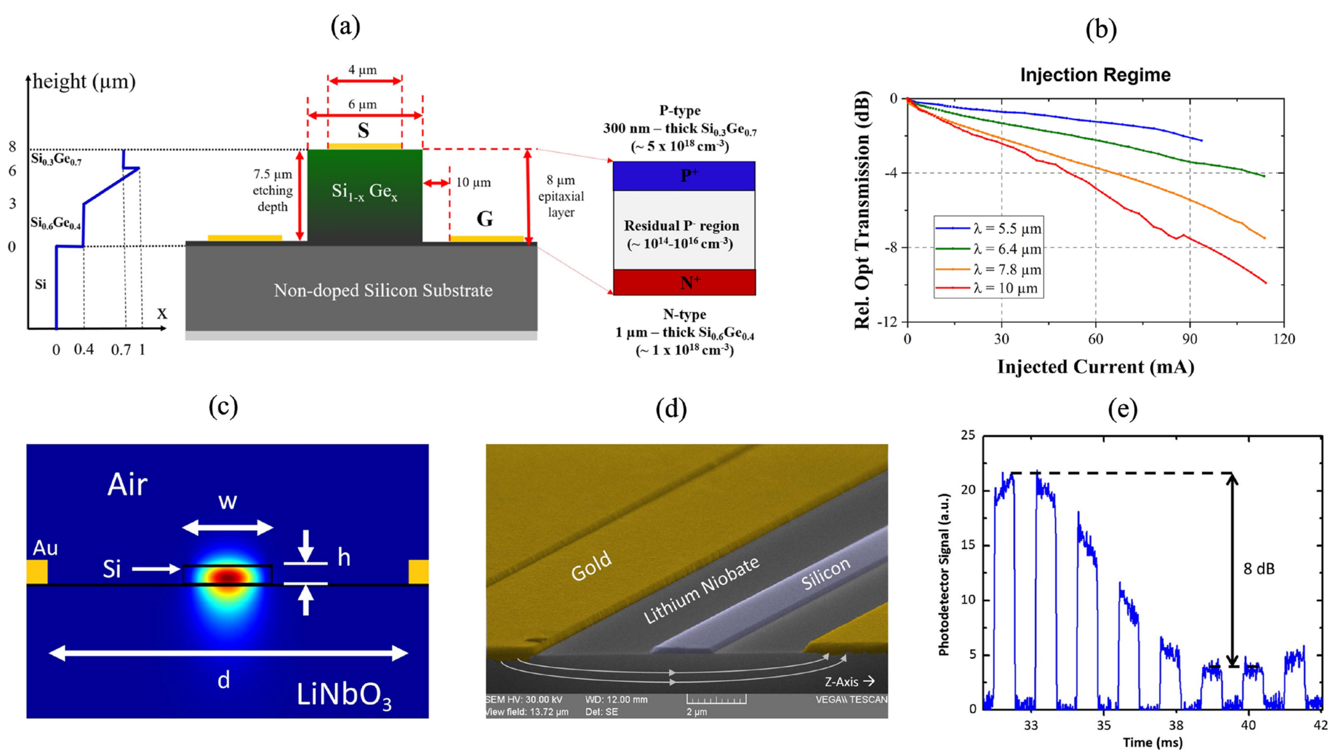

FIG. 5. (a) Cross section of a PIN junction FCPD modulator in a SiGe waveguide, with its Ge content along the growth axis. (b) The static characterization of the EAM in the current injection regime at different mid-infrared wavelengths. (a, b) Reproduced with permission from Nguyen *et al.*, Nanophotonics **13**, 1803–1813 (2024). Copyright 2024 Author(s), published by De Gruyter.[84] (c) Silicon on lithium niobate waveguide modulator cross section and simulated mode profile at a wavelength of 3.39 μm. (d) SEM image of the silicon on lithium niobate modulator. (e) Its low frequency extinction ratio in MZM geometry. (c, d, e) Reproduced with permission from J. Chiles and S. Fathpour, Optica **1**, 350 (2014). Copyright 2014 Optical Society of America.[85]

than EAM has been reported yet, to the best of our knowledge, functioning in the higher range of the mid-infrared band (above 4 μm).

The main challenge in using FCPD for modulators at mid-infrared wavelengths, despite its enhanced effect, lies in the larger waveguides and optical modes, which inevitably reduce the field overlap with the fixed free-carrier modulation region. The doped contact layers, which are in turn larger, also lead to increased optical losses and access resistance, limiting the modulator overall performances. In that prospect, high confinement waveguides such as plasmonic, photonic crystal, or slot waveguides could be interesting alternatives to overcome the latter limitations and have already been successfully employed at telecom wavelengths.[86–89] A detailed report of modulators based on the FCPD effect can be found in Ref. 90.

B. Electro-optic materials

When subject to a strong optical intensity or electric field, certain materials are prone to non-linear optical effects. This is the case in particular for non-centrosymmetric crystalline materials, whose optical index can be tuned proportionally to an applied external electric field. In that case, the Pockels effect is exploited to produce the electro-optical modulation. Alternatively, the Kerr effect, which is proportional to the square of the applied external electric field and present in all material structures, can be used but is often much weaker than the Pockels effect in non-centrosymmetric materials. A particular care to the design and orientation of the electro-optic material and of the waveguides has to be taken, in order to preserve the polarization of the light and benefit from the maximal modulation effect.[91]

In opposition to FCPD, the Pockels effect occurs in the whole material subject to the applied external electric field without the limitation introduced by the access resistance, optical losses in doped layers, or modal overlap with the carrier density modulated region. Moreover, the typical electro-optic material response lies in the femtosecond timescale, much above that of FCPD modulators.[92] Most materials used for electro-optical modulation are ferroelectric oxides (lithium niobate, barium titanate, lithium tantalate, etc.), semiconductors such as III–V compounds having a non-centrosymmetric structure, chalcogenide glasses, and organic polymers.[93]

Regarding the mid-infrared band, efforts were deployed again to use what has already been developed for classical telecom wavelengths. Naturally, that favored lithium niobate devices, which benefits from recent advances in fabrication and processing, and is transparent up to 5 μm. Nevertheless, modulators using lithium niobate have not yet been reported to operate above 3.8 μm. Only one notably high performance device has been reported so far, to the best of our knowledge, using lithium niobate on insulator in MZM together with traveling wave electrodes.[94] It displayed a high extinction ratio greater than 20 dB (in DC) at a 2 μm wavelength, a high electro-optical bandwidth above 22 GHz, a low insertion loss of ~6 dB, and a reasonable driving voltage of 6 V. A few other reported devices using lithium niobate or barium titanate, up to 3.8 μm, were limited in their electro-optical bandwidth and overall performance as well as required high driving voltages of several tens of volts, making them hardly suitable for mid-infrared telecommunications.[85,95] The typical geometry of a Si/$LiNbO_3$ waveguide modulator is reproduced in Figs. 5(b)–5(d), as well as its performance. The performance of modulators based on electro-optic materials is discussed in detail in Ref. 90 as well.

Despite the above-mentioned limitations, electro-optic materials are worth exploring for mid-infrared modulators due to their intrinsic fast response and high modal overlap (the entire waveguide can be made of electro-optic materials). Barium titanate should be investigated further, as its transparency window extends up to 7 μm, and its processing and integration have already been studied. Other materials, such as engineered electro-optic polymers,[96] or chalcogenide glasses[97] are worth the attention as well.

C. Quantum confined Stark effect

The quantum confined Stark effect (QCSE) occurs in QWs when an electric field is applied perpendicular to the plane of the wells. This effect results in a shift of the energy levels of the bound states and a redistribution of the charge densities within the wells, which can be exploited for electro-optical modulation.[98,99] In opposition to the Pockels effect and FCPD, QCSE is a strong but narrowband effect. It has been widely studied and used, particularly in III–V QW semiconductor materials,[100] and more recently in SiGe QWs for their compatibility with silicon photonics for C-band telecommunications.[101,102] At short-wave infrared wavelengths, QCSE is used in interband devices, where the transition occurs between confined states in the valence band and conduction band. When an electric field is applied to those devices, electrons and holes are separated in opposite directions, resulting in a reduction in the oscillator strength. Meanwhile, at mid-infrared wavelengths, unipolar devices are used with intersubband transitions within the conduction or the valence band. Using asymmetrical QWs is then mandatory to enhance the tunability of the intersubband transition with the applied bias. Historically, the first experimental demonstrations of modulation were performed using asymmetrical step quantum wells in the 1990s,[103–105] based on a proposition from Yuh and Wang.[106] Asymmetrical-coupled QWs [represented in Fig. 6(b)] based modulation was experimentally demonstrated soon after.[107,108] Those latter structures have the advantage to provide more flexibility in their design and a higher tunability with respect to the applied electric field than the step quantum well structures, and without charge transfer. This should enable the use of the full potential from the fast intrinsic response time of intersubband devices, which lies in the picosecond regime, without the limitations arising from the carrier transit time. Despite its promising performances, intersubband QCSE-based modulators were not reported before two decades later, when it was successfully used to modulate a QCL internal cavity effective dielectric constant.[109] Again, almost a decade passed before new demonstrations were reported, this time involving true external modulator devices, most of them being in mesa or structured metasurface geometries used as reflective modulators. Using III–V semiconductors, Didier and Dely *et al.* reported a device functioning at a 9 μm wavelength having a −3 dB electro-optical bandwidth of 9 GHz, which was successfully used for free space transmission over 31 m using a Herriott cell. Net data-rates of up to 12.5 Gb/s with a room temperature quantum cascade detector (QCD) were demonstrated using On–Off Keying (OOK) amplitude modulation and up to 30 Gb/s with a cooled Quantum Well Infrared Photodetector (QWIP) detector.[110] The phase modulation capability of the mesa modulator embedding asymmetrical coupled

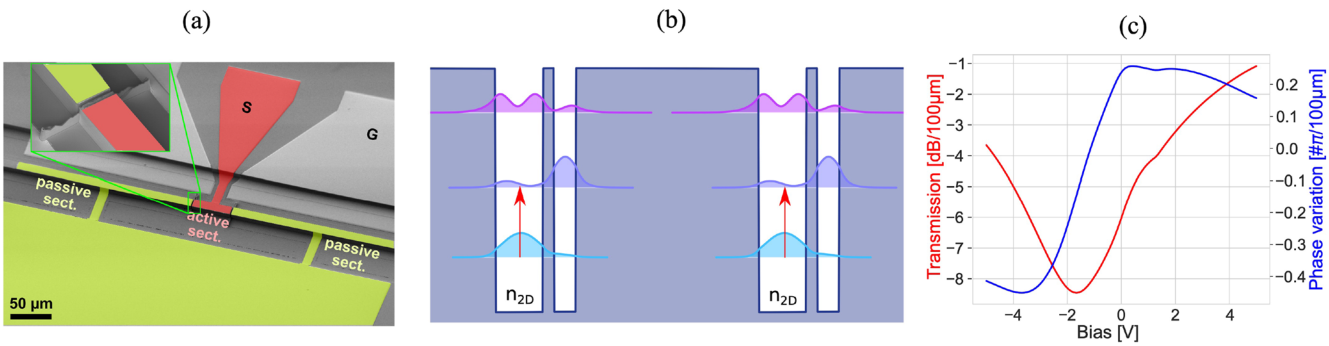

FIG. 6. (a) LWIR QCSE waveguide modulator and based on asymmetrical coupled quantum wells. (b) Two periods of asymmetrical coupled quantum wells embedded within its core. The absorption and phase change of the optical mode propagating through the waveguide is controlled by tuning the applied field across the structure. The right vertical arrow represents the electro-optical transition exploited for the modulation, and n_{2D} is the doping in the larger well. (c) Experimental performance of the device extracted from DC measurements. Reproduced with authorization from T. Poletti, "Optical phase and amplitude modulator and photonic integration for long wave infrared free space optical telecommunications," Ph.D. thesis, Université Paris Sciences et Lettres, 2024. Copyright 2024 Author(s).[113]

quantum wells was also investigated. Dely *et al.* reported a phase modulation of about 5° under a 5 V bias excursion centered near the intersubband transition absorption peak of the device.[111] Using metasurfaces with a similar active structure, Chung *et al.*[112] demonstrated even up to a 60° phase modulation with a 6 V bias excursion on the same material platform. Regarding waveguide geometry implementation, embedding asymmetrical coupled quantum wells in the waveguide core, an EAM with an extinction ratio greater than −14 dB using a 500 μm long waveguide has experimentally been demonstrated recently. The −3 dB electrical bandwidth was measured to be up to 1.4 GHz on a 200 μm long waveguide, limited by the parasitic capacitance of the on-chip electrical access. An extinction ratio up to −7.5 dB/100 μm and a phase modulation up to $0.7\pi/100$ μm under a 5 V bias excursion could also be extracted from measurements.[113] The device geometry and measured performance are reproduced in Fig. 6. In parallel to the above recent developments on InP, the intersubband Stark effect has been investigated using step and triangular quantum wells in the valence band on the SiGe platform, motivated again for its compatibility with CMOS technologies. Theoretical performances are promising and could reach an absorption modulation on the order of 1 dB/100 μm at 7.3 and 10 μm with triangular quantum wells under a 12 V bias excursion and an electro-optical bandwidth on the order of 60–70 GHz for a 100 μm long waveguide.[114]

The recent advance in the developments of modulators using intersubband QCSE showed promising performances. Nevertheless, their implementation in waveguide geometry is still in its infancy and requires further investigations. Only one waveguide modulator using that effect was effectively realized to our knowledge[113] and another simulated performance was reported.[114]

D. Other materials and effects

A few other materials or physical effects are explored for optical modulation in the mid-infrared. The use of two-dimensional materials, such as graphene, shows promising performance and devices functioning from 2 μm to several tens of μm have been theoretically investigated using this material. Nevertheless, the low maturity of graphene-based mid-infrared modulators, especially using plasmonic waveguide structures, faces considerable challenges in their fabrication and integration process. To our knowledge, experimental characterization still lacks. Only one experimental demonstration of a chalcogenide glass based photonic waveguide embedding a double layer of graphene has been reported to the best of our knowledge, functioning in the 2 μm band. The authors reported a modulation depth of 8 dB/mm under a ±5 V bias. Their device was limited in its high speed operation by the access contact, but the authors claim to be able to reach the GHz performance with a high speed dedicated design.[115] A detailed review of graphene based modulators is available in Ref. 90. Another promising effect that has shown great potential for optical modulation is the use of polariton splitting when transitioning from a strong light–matter coupling to a weak light–matter coupling regime. Embedding quantum wells in an optical cavity whose resonant frequency is closely matched to the optical intersubband transition energy in the quantum wells leads to the formation of two distinct peaks in the absorption spectrum of the cavity in the strong light matter coupling regime. Using an external bias to fill or deplete the wells with free carriers allows us to transition in and out of the strong light–matter coupling regime. Pirotta *et al.* demonstrated such a device in the mid infrared (MIR) band using a strip metal–metal resonant cavity used as a reflective modulator. An extinction ratio up to 30% at a wavelength of 9.7 μm has been reported with a −3 dB frequency cutoff of about 750 MHz.[116] A new generation of devices using transition between weak and strong light–matter coupling regimes based on asymmetrical coupled quantum wells has been recently reported by the same group, this time using metal–insulator–metal (MIM) patch antenna resonator arrays. The device showed a −3 dB bandwidth around 8 GHz for a modulation depth in reflection of 0.2 at a 9.6 μm wavelength.[117] Nevertheless, the integration of such devices in a photonic integrated circuit, and especially in waveguide geometry, could be difficult due to the requirements of the strong light–matter coupling regime, which necessitate high optical confinement. Several other approaches are also studied, using phase transition in materials such as VO_2, transparent conductive oxides, or liquid crystal.[118] Those are in a much earlier stage of development and require further research to be considered as viable options for photonic integration in the future.

IV. DETECTORS

A. Mercury-cadmium-telluride detectors

Mercury-Cadmium-Telluride (MCT or HgCdTe) is a versatile compound semiconductor material widely used in various applications such as infrared sensing, communication, and imaging. It has maintained its position as the leading material for mid-infrared detectors for many years, mainly because of its wide tunable bandgap, high optical absorption coefficient, excellent quantum efficiency, and long carrier lifetime. A major step in the development of MCT detectors was first achieved in 1959 by Lawson *et al.*,[119] who demonstrated the ability to control the bandgap of HgCdTe material, opening the way to an unprecedented degree of freedom in the design of detectors operating in the infrared spectrum. By adjusting the composition of the HgCdTe alloy, the detectivity range of the detector can be tailored, ranging from near 1.5 μm to the very long-wavelength infrared, at 30 μm. This semiconductor material could also operate both in photoconductive and in photovoltaic modes. The first significant demonstration of MCT performance was made by Bartlett *et al.*,[120] who achieved the background-limited performance of photoconductors operated at 77 K in the LWIR spectral region, but at the price of a large dark current noise. Subsequent improvements came with advancements in fabrication technology, particularly in the capacity to produce a highly n-doped HgCdTe material. These developments have led to an enhanced device performance, including high quantum efficiency (>65%)[121] and fast response time (several nanoseconds, GHz range), allowing for operation across a broad frequency range.[122] Nevertheless, HgCdTe infrared detector technology encounters various notable limitations, including limitations on array size, substantial dark currents at room temperature due to band-to-band tunneling, and material fragility.[123] Despite that, state-of-the-art Vigo Peltier-cooled MCT detectors can achieve bandwidths of up to 1.2 GHz, along with responsivities of hundreds of mA per watt.[124]

B. Quantum well infrared photodetectors

Quantum Well Infrared Photodetectors (QWIPs) were developed in the late 1980s after the discovery of intersubband transitions and their potential for generating stimulated emission.[125,126] The active region of a QWIP consists of multiple semiconductor layers with varying energy bandgaps, typically GaAs/GaAlAs. The building block is a QW that traps electrons (or free carriers) that can then be promoted to the conduction band by the absorption of an infrared photon. Applying an external voltage tilts the energy levels, allowing the excited carriers to escape the well and produce a photocurrent. As displayed in Fig. 7(a), the short photon lifetime of intersubband transitions enables the device to achieve a high bandwidth of ~100 GHz.[127] By carefully selecting parameters such as well width, barrier height, and well doping density, a QWIP can achieve rapid detection for wavelengths up to 20 μm. To improve absorption, the design incorporates multiple QWs, as the absorption of a single well is strongly limited. Achieving high responsivity requires biasing the detector with a high voltage. A notable characteristic of QWIP detectors, and intersubband devices in general, is that only the TM-component of the incident light's polarization can induce electron scattering between subbands, leading to the detection process. Initial QWIP development was limited to low temperatures due to significant dark current, with a bandwidth around 26 GHz. A major breakthrough demonstrated high heterodyne detection bandwidths at room temperature using a QWIP with 100 QWs operating at ~10 μm.[128] The device, fabricated in a 16 μm side square mesa and illuminated from a 45° polished substrate, exhibited a flat response up to 110 GHz despite its 3-dB cutoff around 25 GHz, highlighting QWIP's high-frequency capabilities. The next advancement involves incorporating a QWIP in an antenna, reducing the active volume without compromising radiation collection or quantum efficiency. In 2001, QWIPs with arrayed patch antenna resonators were proposed, allowing normal incidence illumination and confining the electromagnetic field within a subwavelength volume.[129] This

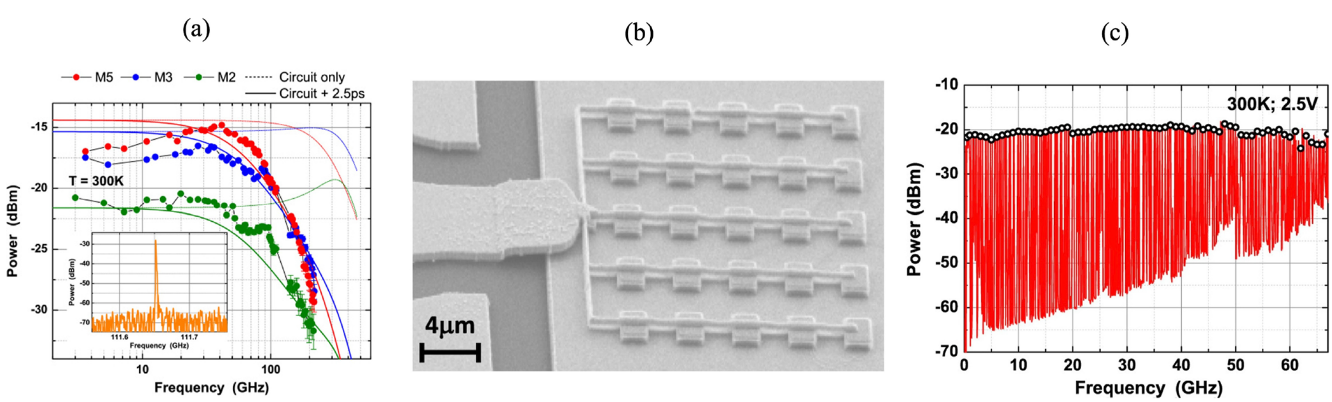

FIG. 7. (a) Room-temperature experimental frequency response of different photodetectors (red dots, blue dots, and green dots) in the frequency bands 0–110 and 140–220 GHz. The measurements are obtained at 10 μm by heterodyne mixing of two single-mode QCLs, whose beatnote close to 110 GHz is shown in the inset. Reproduced with permission from Lin *et al.*, Optica **10**, 1700–1708 (2023). Copyright 2023 Optica Publishing Group.[127] (b) Scanning electron microscopy (SEM) image of a 5 × 5 array of patch antenna resonators integrated with a coplanar waveguide. (c) Heterodyne detection at 10 μm with a nearly flat frequency response up to 70 GHz at room temperature, solely limited by the measurement system bandwidth. Reprinted with permission from Hakl *et al.*, ACS Photonics **8**, 464–471 (2021). Copyright 2021 American Chemical Society.[131]

approach enhances the radiation collection area while reducing the electrical area of the detector, hence resulting in improved high-speed performance and high detectivity [Figs. 7(b) and 7(c)]. The association of patch antenna resonator to heterodyne detection has recently permitted room temperature operation with unmatched sensitivity and speed.[130,131] Recent advancements in patch-array QWIP detectors have showcased a remarkable frequency response of up to 220 GHz through mid-infrared photomixing. At room temperature, these detectors demonstrated an impressive 3-dB bandwidth of ~100 GHz and a responsivity of 80 mA/W.[132] In conclusion, QWIPs, with their high bandwidth and responsivity, are very much effective for high-performance infrared detection applications, especially when combined with advanced antenna designs to enhance their capabilities.

C. Quantum cascade detectors

The QCD, proposed in 2002, was initially made using an InGaAs/AlInAs lattice-matched on InP and utilized a QCL structure as the detector.[133] QCDs feature an electron injector, allowing for zero-bias operation. As a result, these detectors are not constrained by dark current at high temperatures and can operate at room temperature, unlike QWIPs, whose photocurrent is superimposed to a significant dark current. However, QCDs' initial responsivity was relatively low, on the order of μA/W. In 2005, Thales successfully implemented the first enhanced QCD on GaAs/AlGaAs.[134] This development achieved an impressive responsivity of 35 mA/W at a wavelength of ~9.2 μm and a temperature of 50 K. Subsequently, researchers focused on the development of high-speed QCDs,[135] hence demonstrating a bandwidth of 23 GHz along with a responsivity of 33 mA/W at 5.6 μm. Meanwhile, other research focuses have been investigated, such as lower wavelengths,[136] higher wavelengths,[137] and broadband wavelength detection.[138] The development of QCD detectors has at present reached a fairly mature stage, demonstrating an impressive responsivity of above 100 mA/W at room temperature.[113,139] Record external quantum efficiencies (EQEs) of 40% at 80 K and 25% at room temperature have also been reported in the case of a 4.1 μm-QCD embedding a single period active region in a waveguide configuration.[140] In addition, these detectors have potential in achieving a large bandwidth due to their intrinsic fast carrier dynamics, with a notable 25 GHz, while benefiting from a responsivity of 85 mA/W at room temperature.[141] In addition, alternative geometries, such as double QCD detection for spectroscopy applications, have been investigated.[142] Last but not least, the need for monolithic integration has led to the exploration of QCD implementation on different platforms, such as Si[143] or GaN.[144] Detailed discussion about QCD can be found in Ref. 145.

D. Interband cascade infrared photodetector

Similar to QCDs, interband cascade laser structures can also be used as detectors, known as Interband Cascade Infrared Photodetectors (ICIPs). A typical ICIP band structure is shown in Fig. 8. Unlike intersubband detectors, which require careful consideration of the incoming light's polarization, ICIPs can operate with any polarization and from various directions. Initial designs using the same W-QW structure as ICLs showed room-temperature operation on a broad wavelength window up to 4 μm, but with low responsivity (tens of mA/W).[146] Efforts to enhance the ICIP efficiency included adopting superlattice heterostructures, which reduced the Johnson and shot noise by utilizing multistage absorbers. This configuration, involving alternating semiconductor layers with mismatched energy bandgaps, improved carrier confinement and reduced dark current.[147,148] Optimizing absorber thickness and cascade stages further improved the performance, surpassing MCT detectors in high-temperature detectivities.[149] However, large phonon scattering times limit the maximum bandwidth due to Shockley–Read–Hall and Auger recombination processes, although this also results in a higher peak responsivity and a lower dark current compared to QCDs.[150,151] Recent advancements in ICIPs have demonstrated a high responsivity and a wide bandwidth up to 7 GHz and 60 mA/W for wavelengths up to 5 μm.[152] Compared to MCT detectors, ICIPs offer advantages such as lower Auger recombination, reduced tunneling currents, and high growth uniformity.[153] Using ICIPs in FSO communication setups increases design flexibility, allowing a broader range of wavelengths in transmitters and offering fast detection, high responsivity, and high saturation levels when biased.[154]

E. Uni-traveling carrier photodetectors

Uni-traveling carrier (UTC) photodetectors are based on type-II superlattices (T2SLs),[156] which are obtained by stacking InAs and GaSb monolayers on GaSb substrates.[157] UTC photodiodes are based on interband transitions, making them suitable for mid-wavelength infrared detection up to 30 μm. The UTC structure harnesses the rapid electron transport and minimal dielectric relaxation time of the hole carriers, resulting in exceptional device bandwidth performance. Consequently, this technology has found extensive application in the near-infrared band. In terms of performance, UTC and MCT photodetectors demonstrate similar capabilities, with the distinguishing factor being the ability of T2SLs to operate at higher temperatures. However, UTC structures remain prone to high non-thermal noise caused by trap-assisted tunneling.[158] Recent studies have reported a high-performance T2SL InAs/GaAsSb detector operating under a −5 V negative bias and exhibiting a bandwidth of tens of GHz along with a high responsivity of ~300 mA/W.[159,160]

F. Which detectors for FSO applications?

FSO communications rely on using various *ad hoc* detectors to convert optical signals into electrical ones, each with its own advantages and limitations. Table II displays the state-of-the-art performances of the most promising mid-infrared detectors for FSO communications. Photodetectors such as MCT, UTC T2SL, and ICIP stand out for their high detectivity, which is essential for signal recovery due to high losses and dispersion in the propagation channel. These devices also offer a broad frequency range, facilitating implementation of wavelength division multiplexing (WDM) in FSO systems and increased data rates. On the top of that, they do not have strict polarization selection rules, therefore allowing for polarization division multiplexing. However, they do have limitations such as relatively high dark current and limited bandwidth below 12 GHz, while ICIP and UTC T2SL detectors cannot currently detect in the LWIR. In contrast, detectors made with intersubband technology offer unique features, including potential for very large bandwidth (around 100 GHz) and wide wavelength accessibility. However, their strict polarization selection rules and relatively low

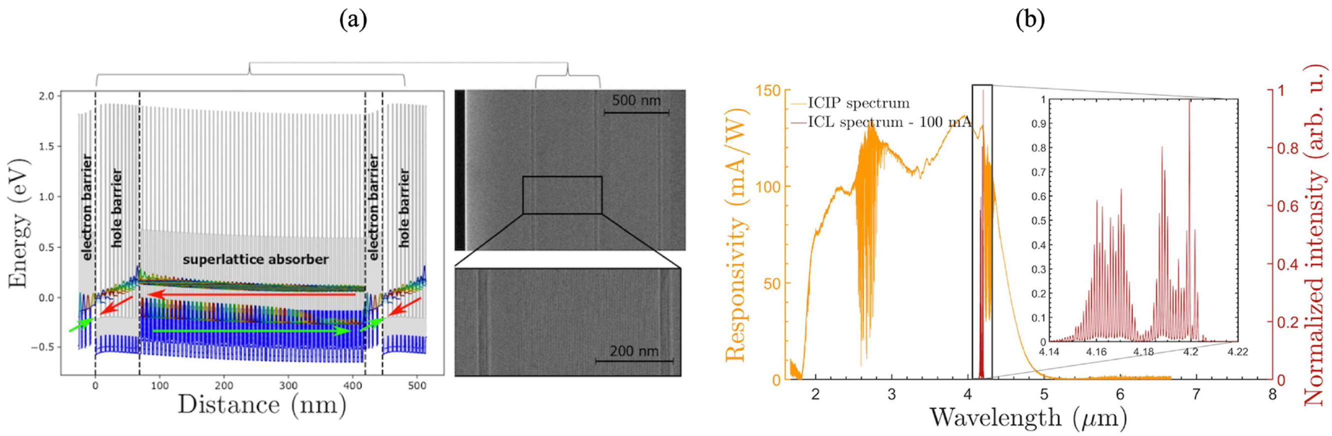

FIG. 8. (a) Schematic representation of the band alignment and SEM picture of the heterostructure of the ICIP detector. (b) Measured responsivity of the ICIP under zero bias operation (yellow) together with the normalized emission spectrum of an ICL at a temperature of 20 °C (red). The detector is well suited for the emission wavelength of the source, around 4.18 μm. Reproduced with permission from Didier *et al.*, Photonics Res. **11**, 582–590 (2023). Copyright 2023 Chinese Laser Press.[155]

TABLE II. Comparison between actual detectors for FSO applications. RT: Room Temperature. TM: Transverse Magnetic.

	QWIP	QCD	ICIP	MCT	UTC T2SL	RCID
Power consumption	High (<W)	None	High (<W)	High (<W)	High (<W)	High (<W)
Operating temperature	RT (300 K)	RT (300 K)	RT (300 K)	Cooled (270 K)	RT (300 K)	RT (300 K)
Cutoff wavelength (μm)	9	10.3	5.5	12	5	4.7
Responsivity (mA/W)	~100	~85	~240	~500	~600	1970
Detectivity (Jones)	NA	~ 10^{11}	3 $\times 10^8$	~ 10^{11}	10^9	3.5 × 10^9
Bandwidth (GHz)	~>90	~25	~7	1	11	~6
Polarization section rules	Yes (TM)	Yes (TM)	No	No	No	No
References	132	141	152	124	160	161

responsivity are drawbacks that can slow down their utilization, in particular for WDM and polarization multiplexing. Despite that, QCDs still offer the advantage of passive operation and extremely low noise characteristics, making them highly suitable for FSO applications where noise is critical. Recently, resonant cavity infrared detectors (RCIDs) have also been proposed.[161] Such detectors can maintain a high external quantum efficiency close to 60% in a narrow spectral bandwidth even when the absorber is very thin, by imposing multiple passes between top and bottom mirrors. The RCID architecture also provides an enhanced frequency response, since photogenerated carriers can be collected more rapidly from a thin absorber. Recently, a high-speed RCID with 7 GHz 3-dB bandwidth was used to demonstrate a room-temperature 5 Gb/s data transmission from a 4.6 μm DFB QCL emitting more than 100 mW. The total link budget reaches more than 20 dB with no pre-amplification. In conclusion, it is crucial to consider the specific advantages and limitations of each detector. Therefore, the choice of a detector should always be carefully evaluated based on system requirements and objectives. In addition, the power consumption is an important consideration for FSO applications. Nevertheless, it is important to note that although some detectors display a promising performance, most of them need to be cooled to work properly. This is less the case for resonant cavities (patch and others). Finally, the commercial availability of detectors can also be an important criterion of choice for end users; in this case, MCT detectors still have a clear advantage over the concurrent mid-infrared detector technologies listed above.

V. HIGH THROUGHPUT DATA TRANSFER

A. MWIR: 3–5 μm

A pioneering demonstration using ICL technology was carried out in the atmospheric transmission window of 3–5 μm with data rates of up to 70 Mb/s and a bit error rate (BER) of less than 10^{-8}.[162] The performance of the FSO link was compared with that of a near-infrared link under various fog conditions in the context of an indoor communication. Although these experiments demonstrated the lower attenuation and scintillation of the mid-infrared FSO link, they were severely limited by the need for cryogenic temperatures, making it impractical for most practical applications. In recent years, the optimization of high-speed link capacity has received a real boost from the use of QCLs. Recent advances have enabled transmission rates of 4 Gbit/s in the 3–5 μm wavelength range, which have subsequently been improved to 6 Gbit/s. These milestones were accomplished using a specific QCL operating at 4.65 μm with a 350 MHz bandwidth. However, achieving faster data rates with direct modulation remains quite challenging due to the limited bandwidth of MCT detectors. A very recent study demonstrated that the combination of a DFB QCL and a RCID detector (see above) can achieve high-quality 2.5 Gbit/s operation with at least 20-dB link budget.[161] Thanks to the strong improvement in the interband cascaded technology, groundbreaking data transmission has been accomplished featuring an ICL at 4.2 μm associated with the ICIP detector as described in Fig. 8. After free-space propagation of around 2 m and implementation of digital signal processing (DSP), On–Off Keying (OOK) transmission capabilities at 12 Gbit/s with a BER of less than 0.4% and 14 Gbit/s with a BER of less than 4% were demonstrated. With PAM4, data transfers were also achieved at 14 Gbit/s with a BER of 0.23% and at 16 Gbit/s with a BER of less than 4%.[155] Last but not least, it was also shown that epitaxial ICLs on silicon (as the one displayed in Fig. 4) demonstrated very promising capabilities for high-speed operation.[53] For example, the eye diagrams shown in Fig. 9 correspond to the data rates of 8 Gbit/s under OOK modulation with a BER of 0.0022% and 10 Gbit/s with PAM4 and a BER of 0.11%, both results being obtained after a 2-m propagation distance.[163] Let us remind that the eye diagram depicts the superposition of the recorded signal at a fixed time interval corresponding to an integer multiple of the bit time-length. Therefore, this tool enables a qualitative assessment of transmission performance, with an open eye indicating a low error rate by showcasing the ability to distinguish between different modulation levels. Altogether, these results are very much encouraging for the development of MWIR free-space communications with direct modulation, particularly those with ICLs that can directly address energy-limited scenarios such as data exchange between satellites or rovers exploring distant planets.

B. LWIR: 8–14 μm

Pioneering activities on free-space optical links established in the mid-infrared wavelength range can be tracked back to the late 1960s.[164–166] In 1977, McElroy and co-workers at NASA developed a laser communication system for satellite-to-ground data transmission employing a 10-μm CO_2 laser module and an MCT photomixer cooled at cryogenic temperatures.[167] The system was capable of operating up to 300 Mbps data transmission rates. Despite the capability to reach a high output optical power, the interest in FSO systems based on CO_2 lasers has progressively declined due to their bulky dimensions and complex implementation. In 2001, subsequently to the development of quantum cascade technology, the first demonstration employing a directly modulated QCL in the LWIR showed successful free-space transmission of 2.5 Gbit/s at 8.1 μm at a laser operating temperature of 85 K and a liquid nitrogen-cooled QWIP detector.[168,169] The same year, another group further succeeded in establishing a transmission link using QCLs operating at 9.3 μm over a distance of almost 10 m, achieving a data rate of 115 kbit/s.[170] Notably, even when the external link was extended to a propagation distance of 300 m under foggy conditions, the transmitted output power remained stable at around 80% of the back-to-back value. This observation was truly a first of its kind, proving the resistance of the 9.3 μm wavelength to the negative effects caused by humidity. Since then, however, progress in pushing the limits of data speed has been hampered by limitations associated with cryogenic QCL operation. In 2019, a major milestone was reached with the demonstration of 1 Gbit/s transmission at room temperature using direct modulation at 10.6 μm.[171] A breakthrough showed 11 Gbit/s transmission at 9.6 μm using direct modulation QCL coupled with computer-aided processing to improve the QCD performance.[172] Another demonstrated a 9.1 μm directly modulated QCL at 20 °C achieving 7 GBaud PAM6, 9 GBaud PAM4, and 15 GBaud Non-Return-to-Zero (NRZ), in compliance with the advanced error correction technique limit [Fig. 10(a)].[173] In this study, different detectors were considered, including MCTs, a passive QCD, and metamaterial-patterned detectors. Different modulation formats, such as PAM and DMT (discrete multi-tone) signals, were also considered. Using a 9.15 μm directly modulated QCL and a MCT detector, DMT transmissions of up to 5.1 Gbit/s and PAM8 transmissions of up to 8.1 Gbit/s were achieved. In addition, a configuration with a 9.6 μm directly modulated QCL and a fully passive QCD enabled transmissions of up to 11 Gbps.[173,174] Recently, the same team has achieved a remarkable breakthrough by reporting a record-breaking bit rate exceeding 55 Gbit/s NRZ signal from a directly modulated DFB QCL.[175] This result was accomplished using a QCL with an enhanced RF design, along with two high-speed detectors incorporating meta-materials to boost responsivity. That said, it is important to stress that these experiments were made on a very short transmission distance (a few centimeters)

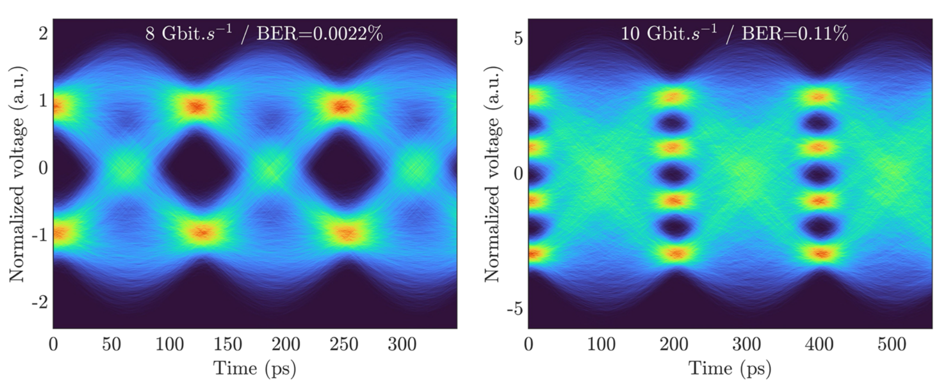

FIG. 9. Measured eye diagrams of a MWIR ICL transmission after a free-space propagation of ~2 m, for two distinct modulation formats: (left) OOK at 8 Gbit/s, demonstrating a BER of 0.0022%, and (right) PAM4 at 10 Gbit/s with a BER of 0.11%. Equalization allows us to significantly enhance the quality of the transmission. Reproduced with permission from Kim *et al.*, APL Photonics **9**, 106103 (2024). Copyright 2024 Author(s), published by AIP Publishing.[163]

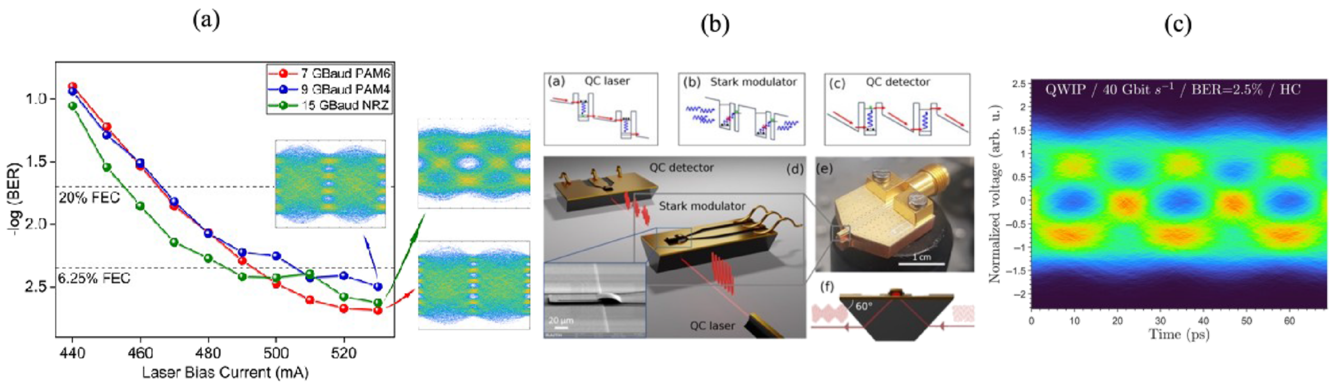

FIG. 10. (a) BER results as a function of laser bias for different modulation formats at 20 °C. Insets: Selected eye diagram for 7 GBaud PAM6, 9 GBaud PAM4, and 15 GBaud NRZ. Reproduced with permission from Joharifar *et al.*, Opt. Express **32**, 29138 (2024). Copyright 2024 Author(s), published by Optica Publishing Group.[173] (b) Comprehensive unipolar quantum optoelectronic system, operating at 9.3 μm, featuring a QCL, a QCSE modulator, and a QCD. The detector can be replaced by a QWIP for an enhanced performance. Reproduced with permission from Dely *et al.*, Laser Photonics Rev. **16**, 2100414 (2022). Copyright 2022 Author(s), published by Wiley-VCH GmbH.[176] (c) Eye diagram of the transmission after a 31-m free space propagation at 40 Gbps using a QWIP. Reproduced with permission from Didier *et al.*, Adv. Photonics **4**, 056004 (2022). Copyright 2022 Author(s) under CC BY 4.0 license, published by SPIE and Chinese Laser Press.[110]

and use quite a lot of DSP. Although the latter is necessary, it is also known that higher speeds require more complex DSP, which may create higher latency, undesirable for widespread telecommunications applications. In addition, there is a lack of data on performance in real-world outdoor environments, especially under conditions involving turbulence or fog. Analyzing the pros and cons of using LWIR lasing wavelengths for FSO communication is essential to unlock its potential. One key advantage of LWIR is that, at longer wavelengths, absorption and scattering tend to be of similar magnitudes, unlike shorter wavelengths where scattering dominates. Although absorption might initially seem like a major drawback, potentially limiting transmitted power, the situation is more nuanced. When we treat both scattering and absorption as probabilistic events, photons that interact more with water particles are more likely to be absorbed. This means that absorption primarily affects scattered photons, leaving the ballistic photons—the ones that travel in straight paths—largely unaffected. The ballistic nature of photon transmission presents a significant advantage in using LWIR for FSO communications. When transmitting pulses, a ballistic flux reduces temporal elongation, which is common in scenarios dominated by scattering. This, in turn, minimizes intersymbol interference, a key factor that can directly limit the data rate in telecommunications. By preserving the shape and timing of transmitted pulses, LWIR wavelengths can thus potentially enable higher data rates compared to shorter wavelengths where diffusion is more prevalent.

In order to further overcome bandwidth limitations, external modulators remain the best candidates for improving the FSO performance, especially moving forward to coherent communications. Using an external modulator allows increasing both the speed and the range of the transmission links. Unprecedented data rates reaching 10 Gbps have been attained utilizing unipolar quantum optoelectronics, which incorporates a QCL, a Stark modulator, and a QCD operating within the thermal infrared window [Fig. 10(b)] at 9.1 μm.[176] This work has been even pushed further by using pulse shaping, DSP, and a nitrogen-cooled QWIP detector. As shown in Fig. 10(c), a record bit rate of 40 Gbps was achieved for OOK and PAM4 modulation schemes after a 31-m propagation in free space along with a BER compatible with error-correction codes.[110] Assuming an output power of 30 mW, experiments revealed that around 4 mW is enough to detect a signal and receive the message. In order to give a rough estimation of the power budget, in a situation where visibility drops to 1 km (fog), the attenuation due to scattering jumps to 3.3 dB/km, which is still much lower as compared to equivalent scattering at 1.5 μm (9.3 dB/km) and 4 μm (5.4 dB/km). In a very recent study, it is shown that the performances of both modulators and detectors can be drastically improved by embedding them into metamaterials. For doing so, metamaterials have to be engineered differently as the role of light–matter interaction must be properly controlled in the two devices. Metamaterial-enhanced performances allow the realization of data transmission with a record rate of 68 Gbit/s, which is the record achieved with such a technology.[177]

C. SWIR-to-MWIR non-linear conversion

An alternative to the above-mentioned demonstrations, which relies on active and passive photonic components developed specifically for MWIR wavelengths, is to take advantage of the widely available, mature, and high performance components developed for SWIR wavelengths, in particular near 1.5 μm, and convert the optical signal in the SWIR directly to the MWIR range. A first way to produce MWIR photons from a SWIR source is through photon downconversion, where the SWIR photons of a commercially available laser source are converted to MWIR photons through non-linear processes such as difference frequency generation (DFG) in crystals such as (doped-)periodically poled $LiNbO_3$ (PPLN) or $KTiOPO_4$. The mid-infrared signal can be either detected at the receiver side with mid-infrared MCT detectors,[178] or up-converted again to the SWIR through the reverse non-linear process, the sum frequency generation (SFG). Commercially available InGaAs[179] or Si-based detectors[180] can then be employed. This way of generating

MWIR photons from SWIR ones is mostly dedicated to a narrowband optical signal. Therefore, another field of research is the generation of broadband optical signals in the SWIR range, which are then converted to the MWIR range. In that case, the photon conversion from the SWIR to the MWIR is achieved from four-wave mixing (FWM),[181] cross-phase modulation (XPM),[182] and optical parametric amplification (OPA).[183] The latter approach facilitates the use of WDM techniques to increase the capacity of mid-infrared links, using mature components developed for the SWIR band and extensively optimized for high-speed modulation,[184] or supporting advanced modulation formats such as phase modulation or orbital angular modulation (OAM).[185] One early successful demonstration of effective wavelength conversion from 1.5 to 3.8 μm was conducted by Cho *et al.*[186] with a pair of Ti:PPLN-based integrated nonlinear wavelength converters. They studied the transmission of a 160 Mbit/s return-to-zero quadrature phase-shift-keying (RZ-QPSK), and subsequent research has shown the possibility of transmitting Gbit/s signals using the same methods. A recent breakthrough demonstrated the use of the high-capability 1.5 μm range to transmit signals in the 3–5 μm window by combining WDM, mode-division multiplexing (MDM), and OAM (cf. Fig. 11). This study employed three wavelengths around 3.4 μm (3.396, 3.397, and 3.398 μm, respectively) on a single polarization, with each wavelength carrying two OAM beams. By transmitting 50 Gbit/s quadrature phase

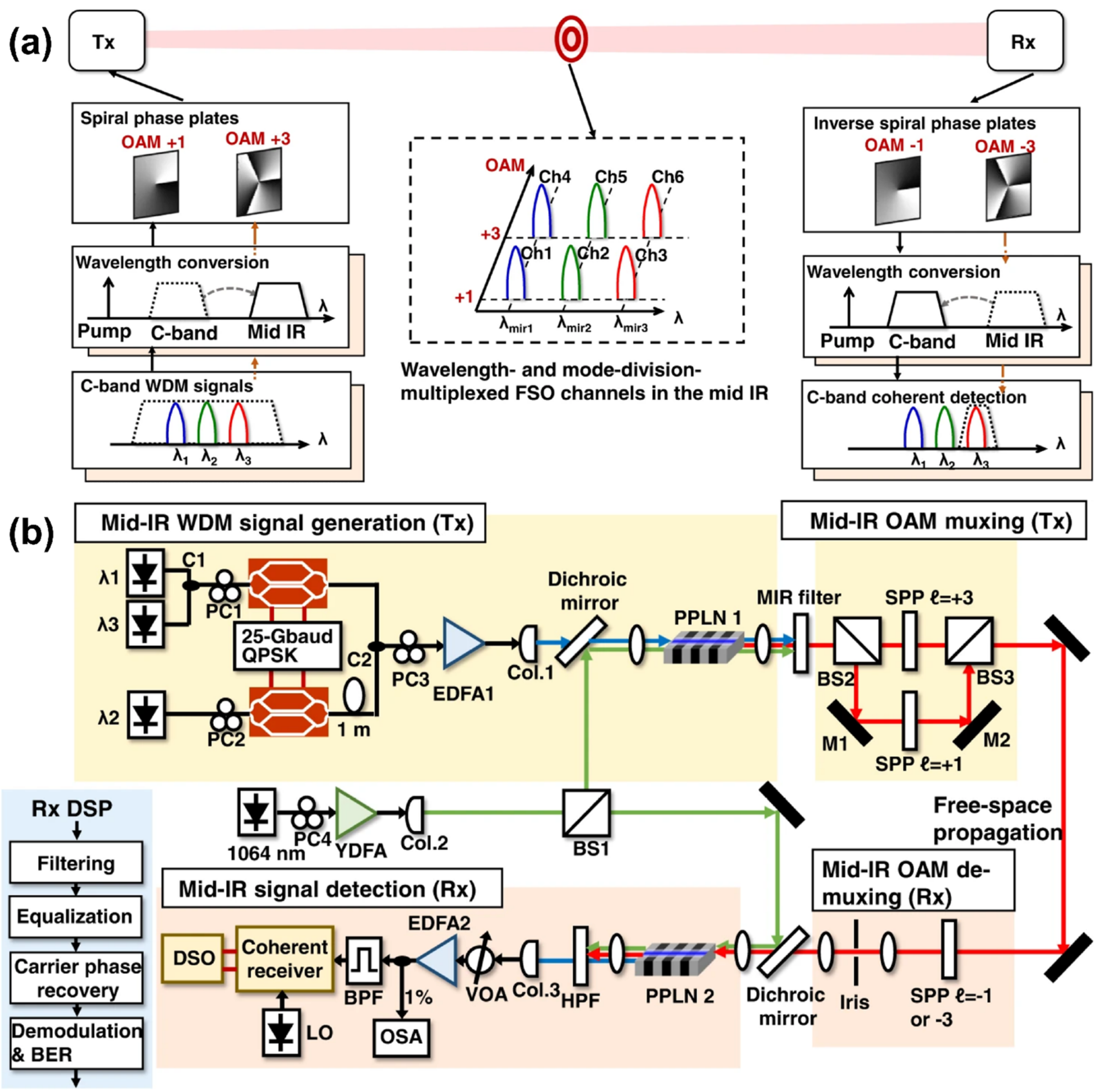

FIG. 11. (a) Concept and (b) experimental setup employing the SWIR-to-MWIR non-linear wavelength conversion, WDM- and OAM-based mode-division-multiplexing to implement a high-speed free-space optical communication link. Reproduced with permission from Zou *et al.*, Nat. Commun. **13**, 7662 (2022). Copyright 2022 Author(s) under CC BY 4.0 license, published by Springer Nature.[187]

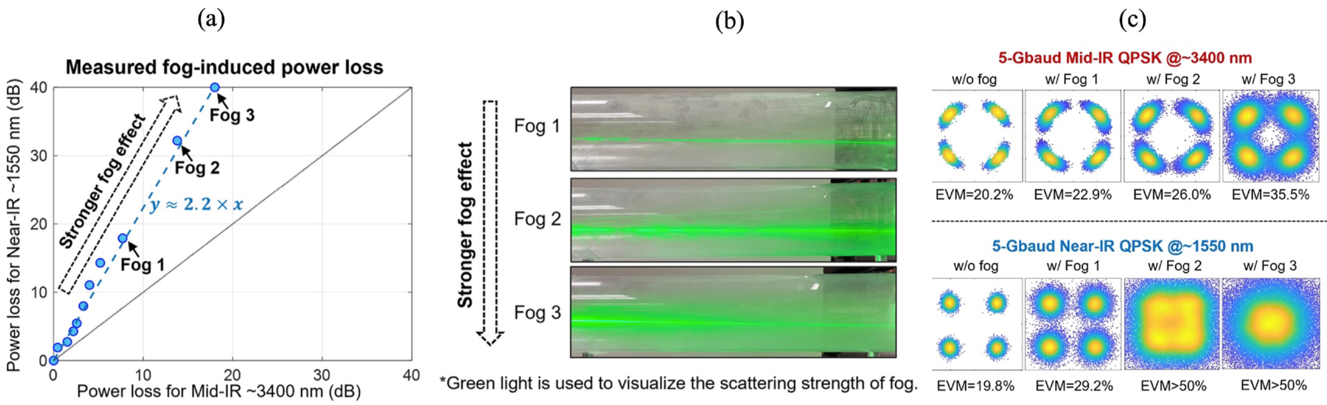

FIG. 12. (a) Power loss caused by fog at 1.5 μm vs at 3.4 μm. (b) Images showing the propagation of a green-light beam through three distinct fog conditions as measured in (a). (c) Data constellations and Error Vector Magnitudes (EVMs) for 2 Gbaud and 5 Gbaud QPSK data channels under clear conditions and various fog scenarios. Reproduced with permission from Zhou *et al.*, J. Lightwave Technol. **42**, 3989–3996 (2024). Copyright 2024 IEEE and Optica Publishing Group.[188]

shift keying (QPSK) data on each frequency with different angular momenta, a total data rate of 300 Gbit/s has been achieved.[187]

Recently, the same group demonstrated an OPO-based, 10-Gbit/s QPSK MWIR data transmitter in an FSO communication link through fog at 3.4 μm,[188] enabling phase-encoded data modulation and coherent reception. The link demonstrated BERs below the 20% FEC limit under fog, causing ~18-dB MWIR power loss, equivalent to roughly 40-dB loss for 1.5 μm as displayed in Fig. 12(a). In order to visualize the effects of fog on a laser beam, Fig. 12(b) illustrates the propagation of a green light beam through three distinct fog conditions, as reported in Fig. 12(a). Figure 12(c) shows the corresponding data constellations and error vector magnitude (EVM) for 2 Gbaud and 5 Gbaud QPSK data channels under clear conditions and various fog scenarios. Despite these promising results, it has to be stressed that non-linear wavelength conversion from near-infrared to mid-infrared still faces some limitations, such as low output power, high power consumption, low efficiency, operation in the sub-4-μm region because of the limited transparency region of typical non-linear crystals currently employed, and the need for expensive and bulky periodically poled lithium niobate devices. Extending the wavelength range to the above 4 μm, to LWIR, could be possible using orientation-patterned (OP) semiconductors with high non-linear coefficients such as GaAs[189–191] or GaP.[192–194] In particular, thanks to its lattice constant and thermal expansion coefficient very close to those of silicon, OP-GaP can be an attractive material for compact mid-infrared integrated photonic circuits on silicon or SiGe platforms. Despite these challenges, ongoing research aims to overcome these limitations and unlock the full potential of non-linear wavelength conversion for achieving extremely high data rates in the mid-infrared range.[187,195]

D. Summary

Data transmission at longer wavelengths has been investigated by many research groups around the world. In the past decade, the number of research articles has significantly increased, demonstrating a truly and active interest in the field. In this paper, we mainly focused our analysis on demonstrations established in the 3–12 μm wavelength range. It is worth mentioning, however, that experiences of data transmission have been successfully conducted in the THz domain as well,[196] but a thorough discussion of this subject is out of the scope of our analysis. Figure 13 shows a summary of the major performance in high throughput data transfer using direct or external modulation of QCL/ICL and non-linear wavelength conversion approaches realized in the MWIR and LWIR atmospheric transmission windows, whereas Table III displays the corresponding comparison between these techniques. Advances in the RF design of mid-infrared technologies have enabled the consideration of direct modulation for both ICL and QCL transmission applications. Currently, the only sources capable of providing high-speed transmission in the 8–14 μm wavelength range are QCLs that support direct modulation or can be used with an external modulator. Indeed, as aforementioned, long-wavelength ICLs are still working at cryogenic temperatures. Considering an external modulator for high throughput free-space data transmission is particularly interesting because of the output power associated with a high modulation power. It can be used for atmospheric layers crossing or between space to ground links. Despite recent efforts to decrease the power consumption of QCLs, it remains quite significant. Conversely, ICLs are highly energy-efficient sources capable of providing high-speed free-space transmission. Last but not least, although wavelength conversion technology is promising due to its ability to access high frequencies and support different modulation formats, it still faces certain limitations. One of the main challenges is insufficient output power in the mid-infrared, limiting its practical implementation. In addition, frequency conversion devices often consume a lot of power, hindering their widespread adoption.

E. Private communications

Despite the numerous advantages of FSO communication, it is also crucial to address the inherent security concerns associated with the physical layer. By employing advanced encryption techniques and secure key exchange protocols, it is possible to enhance the confidentiality and integrity of data transmitted over FSO links.

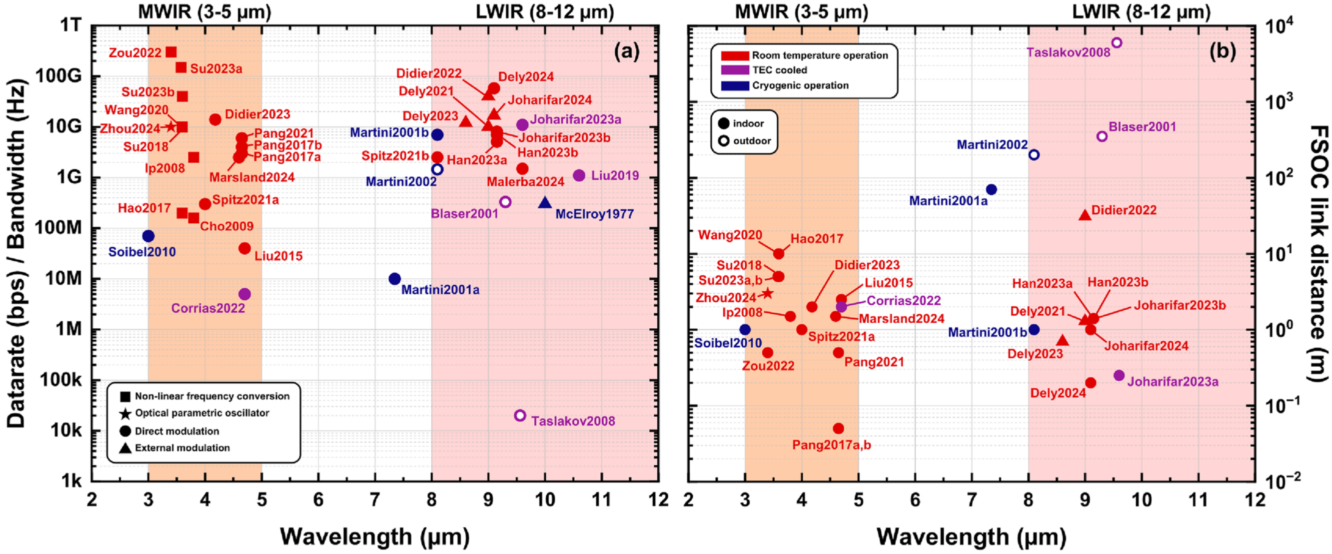

FIG. 13. Summary of MWIR and LWIR FSO demonstrations showing (a) the maximum achieved data rate/bandwidth for each work and (b) the corresponding reported link distance. Indication on the technique used to implement the mid-IR FSO link is given (non-linear wavelength conversion, optical parametric oscillator, and direct or external modulation with native mid-infrared devices), as well as the operation temperature and whether the link was established indoor or outdoor (real atmospheric conditions).The list of selected studies is non-exhaustive, but it gives a fair overview of the main achievements obtained up until now. Details of the selected studies can be found in Refs. 110, 117, 155, 161, 162, 173, 176, 167, 168, 170–172, 175, 186–188, 195, 197–210, and 215.

TABLE III. Comparison between different mid-infrared modulation techniques. DM: Direct Modulation. EM: External Modulation. NLFC: Non-linear frequency conversion. AM: Amplitude Modulation. PM: Phase Modulation. FM: Frequency Modulation. OAM: Orbital Angular Modulation. WDM: Wavelength Division Multiplexing.

	DM ICL	DM QCL	EM QCL	NLFC
Power consumption	Low (<W)	Medium (~W)	High (>W)	Very high (>W)
LWIR accessibility	No	Yes	Yes	No
Modulated output power	Low (~10 mW)	Medium (~50 mW)	High (~100 mW)	Very low (~1 mW)
Reliability	High	High	Low	Medium
Integration	Easy	Medium	Complex	Very complex
Potential bandwidth (GHz)	Low (~5 GHz)	Very large (~100 GHz)	Very large (~100 GHz)	Very large (~100 GHz)
Modulation format	AM	AM	AM/PM	AM/FM/OAM/WDM
Maximum data rates (Gbit/s)	14[155]	58[175]	40[110]	300[187]

Although quantum communications are currently under considerable improvements in performance, they are not applicable to the mid-infrared range, where quantum hardware does not yet exist. For years, it has been demonstrated that photonic chaos can be utilized for data security, random number generation, and even optical radars.[216] The unpredictable nature and complexity of the strange attractor make chaos a powerful tool for developing secure free-space mid-wave infrared communications, enhancing physical-layer security such that eavesdroppers cannot decipher intercepted messages. Several encryption methods have been studied, with the emphasis on the fact that chaos is the medium in which the message is perfectly hidden. The security key of the system relies on chaos synchronization (or anti-synchronization) between a transmitter and a receiver. This technique is well established in the field of fiber optics,[217] where the latest developments demonstrated impressive results such as a 100 Gb/s coherent chaotic optical private communication over 800 km fiber transmission.[218] Chaos synchronization is achieved if and only if the same hardware is used. This means, for example, using identical lasers and detectors with similar electro-optical properties to preserve the characteristics of the chaotic envelop during propagation. Nevertheless, atmospheric impairments can also be detrimental to the chaotic carrier. In 2021, an indoor MWIR private communication based on chaos enciphering was for the first time successfully performed between two matched DFB QCLs at 5.6 μm.[219] In 2024, the same group reported the first-ever data encryption in the LWIR with QCL's photonics chaos at room temperature, extending the communication range to 31 m.[220] Figures 14(a) and 14(c) indeed show that the signal directly

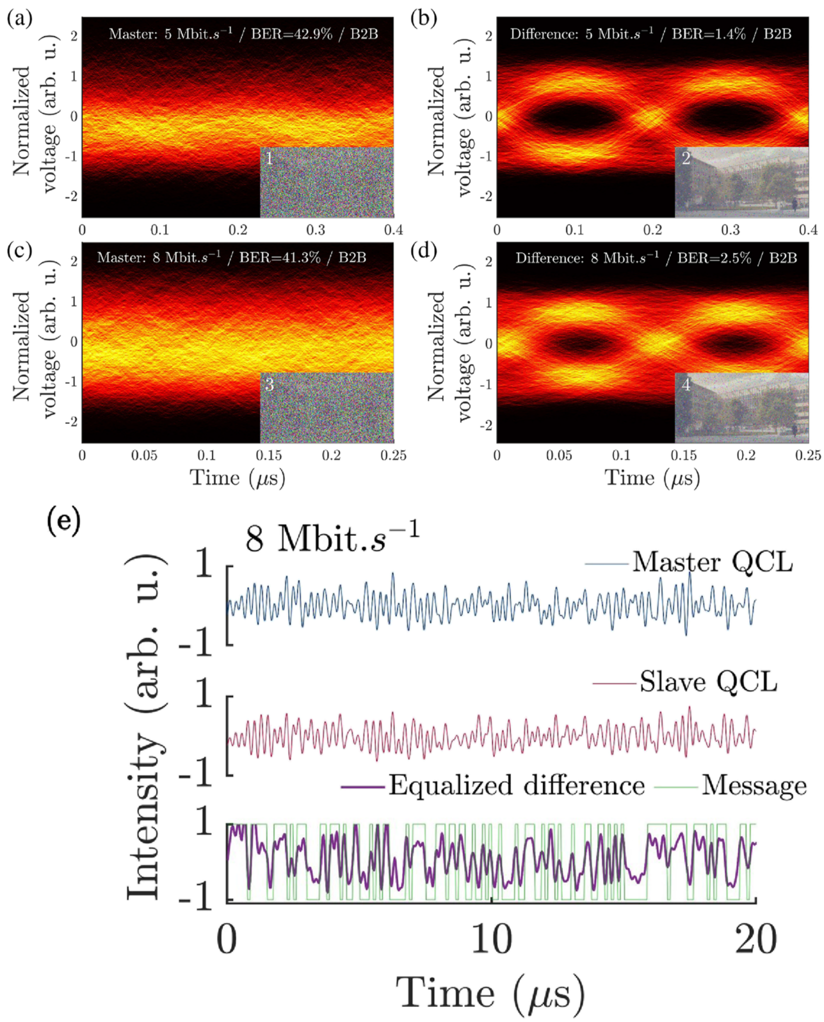

FIG. 14. (a) Master signal exhibiting an error rate of about 43% and (b) difference signal exhibiting an error rate of 1.4%. Eye diagram for 8 Mbit/s transmission. (c) Master signal exhibiting an error rate of 41.3% and (d) difference signal exhibiting an error rate of 2.5%. (e) Experimental time traces for the 8 Mbit/s transmission: (blue) master signal, (red) inverted slave signal, (green) original message, and (purple) equalized difference. Details in the text. Reproduced with permission from Didier *et al.*, Optica **11**, 626 (2024). Copyright 2024 Optica Publishing Group.[220]

retrieved at the receiver is indecipherable. Meanwhile, the legitimate receiver as shown in Figs. 14(b) and 14(d) benefits from a low BER below 4%, enabling error-free transmission after forward error correction, or even a decipherable picture without error-code correction. The insets display the results of the attempted private transmission, where the information encoded in each pixel is converted into a bit stream representing the transmitted message. At the receiver end, the retrieved bit stream is transformed back into an image format. For both data rates, the image remains imperceptible to an eavesdropper who directly detects the laser signal, as demonstrated in Figs. 14(a) and 14(c), highlighting the effective containment of the information. When analyzing the difference signal as in Figs. 14(b) and 14(d), the low BER allows for successful recovery and visual representation. Figure 14(e) displays in the time domain, after appropriate filtering and normalization, in blue the master signal, in red the slave signal, in green the original message, and in purple the difference signal. The message is a NRZ pseudo-random binary sequence (PRBS). Although current data rates are limited to a few Mbit/s, there is significant scope for optimization, in particular to improve the QCL chaotic bandwidth to meet the requirements of higher data rates of 100 to 200 Mbit/s.[221] Promising applications for this technology include communication between ground stations or vehicles and aircraft, as well as providing communication and detection capabilities in harsh environments such as maritime and foggy conditions.

VI. PERSPECTIVES

A. Integrated mid-infrared photonics

Silicon is a highly versatile material widely used in integrated photonics due to its excellent optical properties. At the present time, silicon photonics allows the development of efficient turbulence compensators at 1.55 μm. The implementation of such a system consists of a re-programmable mesh of electrically tunable Mach–Zehnder interferometers directly integrated on silicon.[222,223] The signal compensation algorithm associated with the photonic processor allows for the restoration of the optical signal power even in the presence of strong turbulence, which is a promising advancement for the development of free-space optical communications. The same approach could be easily extended to the MWIR and LWIR ranges, in order to realize complex mid-infrared reprogrammable PICs with many independently tunable beam couplers (e.g., thermally tunable MZIs), on low-loss photonic integrated platforms such as silicon or InP. This would unlock the potential of on-chip photonic analog processing in the LWIR, which is not possible with current PIC technology. This will enable the generation, manipulation, and detection of arbitrary optical beams in the mid-infrared.

Owing to silicon's optical absorption properties, the use of Si-based platforms confines the spectral range of mid-infrared photonic integrated circuits to wavelengths below 8 μm. To overcome this limitation, heterogeneous integration is employed, enabled by techniques such as direct wafer bonding,[224] micro-transfer-printing technology,[225] direct growth of III–V materials on silicon,[226] or flip-chip bonding.[143] Although alloying SiGe has demonstrated reasonable transparency in the 8–14 μm wavelength range,[227] integrating these materials through the above-mentioned techniques remains essential for advancing the performance and extending the operational wavelengths of mid-infrared photonic devices. The mid-infrared silicon platform offers several advantages. First, it supports cost-effective and scalable manufacturing, leveraging the well-established infrastructure of silicon photonics. Second, it enables the integration of mid-infrared functionalities with existing silicon photonic components such as low-loss waveguides, modulators, and detectors. Third, the silicon platform presents opportunities for seamless integration of mid-infrared devices with complementary metal–oxide–semiconductor (CMOS) electronics. Several research groups have successfully implemented mid-infrared devices on this platform, including ICLs,[51,52] QCLs,[51,224] QCDs,[228] and SiGe waveguide modulators.[229] However, a significant challenge arises from the lattice mismatch between materials, leading to dislocation problems that can easily degrade device performance.[226,230,231] Overcoming this issue requires meticulous engineering and optimization of the heterostructures to mitigate the impact of dislocations and improve the long term reliability of the components. To enable industrial applications, achieving full integration on a photonics platform is crucial. The implementation of monolithic integrated components offers several advantages, such as increased miniaturization, improved reliability, and scalability. By consolidating all necessary elements on a single photonic platform, better control over system parameters can be achieved, leading to enhanced efficiency and low costs. Prior studies have demonstrated the successful use of lasers[232,233] and waveguide gratings[234–236] on InP, showcasing an impressive performance. Recent studies have demonstrated the possibility to simultaneously implement several required devices on the same InP platform.[237–239] These materials have the advantage of achieving low background doping levels, below 10^{15} cm^{-3}, either by maintaining low impurity levels or through the use of doping compensation techniques. Absorption losses in bulk structures can be effectively minimized, staying well below 1 dB/cm.[232,240,241] Therefore, it can enable the development of efficient and high-performance devices such as lasers, modulators, detectors, and integrated photonic circuits operating in the mid-infrared range. Concerning monolithic integration of quantum cascade components on the InP platform, an original approach based on bifunctional material has been proposed by Schwarz *et al.*[142,242] This approach, named QCLD for Quantum Cascade Laser/Detector, combines the lasing functionality of a QCL and the detection functionality of a QCD that share the same epitaxial structure. Switching between the two operations is possible by simply changing the applied bias of the device. Until now, this approach has been successfully employed in the case of lab-on-a-chip platforms[29,243] possibly in combination with plasmonic waveguides,[244,245] but the same concept could also be used to implement monolithically integrated transceiver modules for mid-infrared FSO communications thanks to low-loss butt-coupled waveguides.[246] Figure 15 displays some examples of photonic integration for mid-infrared applications including, but not limited to, a 16-channel phase-locked quantum cascade amplifier array,[247] ring quantum cascade resonators with active directional couplers,[239] a monolithic wavelength beam-combined QCL array with integrated waveguide gratings,[248] a monolithically integrated QCLD for lab-on-chip sensing,[243] passive low loss waveguide structures on an InGaAS/InP platform,[241,249] and homogeneous integration of QCL on top of passive InGaAs/InP waveguides with vertical coupling through tapered sections.[232]

Another meaningful possibility is to leverage the ease of generating a frequency comb in QCLs[14,239,250] for multi-wavelength modulation. This approach involves separately modulating the teeth of the comb, which can significantly increase the data rate of the FSO link. The stability and power optimization of the teeth will need to be addressed. By independently controlling the modulation of each wavelength, multiple data streams can be transmitted simultaneously, substantially enhancing the overall capacity of the FSO communication system. Mid-infrared FSO communication offers significant advantages due to its broad window transparency, spanning from 3 to 5 and 8 to 14 μm. This allows for extensive transmission bands, accommodating hundreds of wavelengths simultaneously. In contrast, communication in the SWIR is limited to a narrower band of ~0.3 μm. The mid-infrared FSO system supports a remarkable 20-fold increase in available wavelengths compared to SWIR, promising high-speed and efficient data transmission in future FSO networks.

B. Coherent communications

Coherent communications describe systems that use the phase of the optical signal to encode the information. One widely used format is the Quadrature Amplitude Modulation (QAM) format, which encodes the information on both the phase and the amplitude of the optical carrier. This allows for higher spectral efficiency compared to using only amplitude or phase modulation alone, while being more robust to noise sources at constant bit per symbol. To perform QAM modulation, a general procedure consists in first splitting the optical carrier into two identical beams. In photonic integrated circuits, that can be performed using a Multi-Mode Interferometer (MMI), or any other integrated beam splitter, as shown in Fig. 16.

The first beam undergoes direct amplitude modulation using an external EAM or, as in the general case presented in Fig. 16, using two phase modulators in a Mach–Zehnder configuration. The second beam passes through two external modulators: the first modulates the beam in amplitude like the first beam, and the second introduces a phase shift to achieve a 90° phase offset. The two beams are then recombined, generating a QAM signal with two amplitude modulated signals offset by 90° in phase. To facilitate demodulation, it is necessary to compare the received signal to a reference of phase.

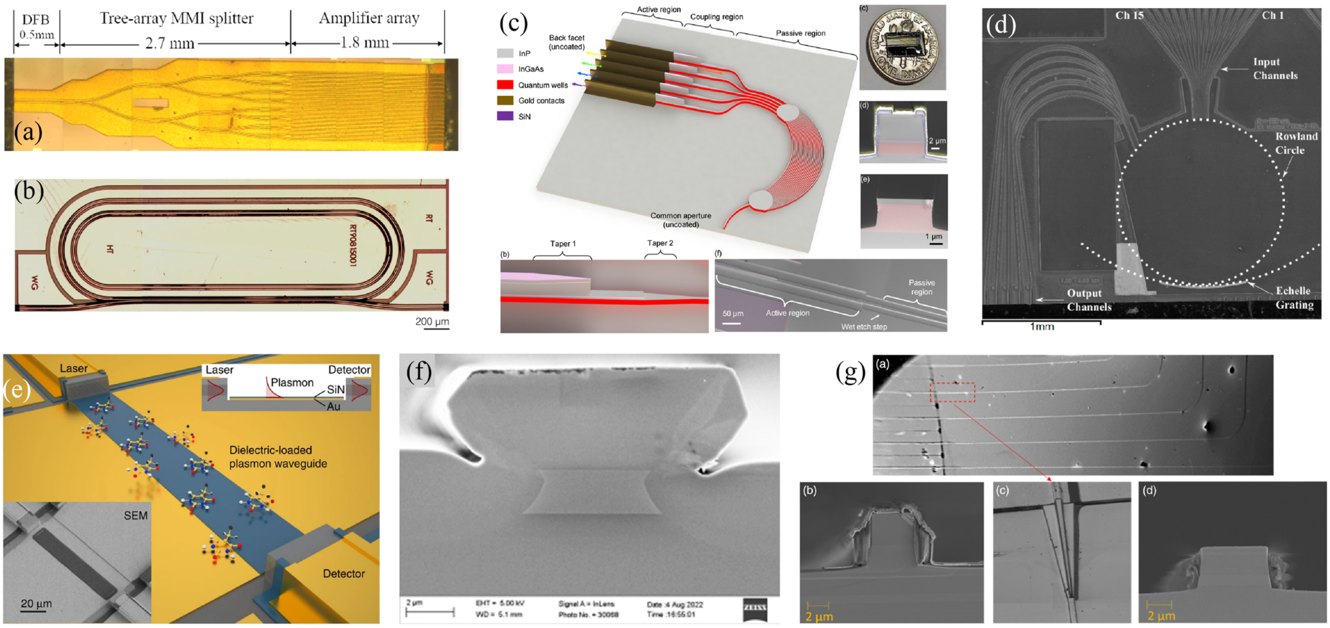

FIG. 15. Examples of mid-infrared photonic integration: (a) 16-channel phase-locked quantum cascade amplifier array (Reproduced from Zhou *et al*., Sci. Rep. **8**, 14866 (2018). Copyright 2018 Author(s) under CC BY 4.0 license, published by Springer Nature);[247] (b) ring quantum cascade resonators with active directional couplers (Reproduced from Kazakov *et al*., Nat. Commun. **15**, 607 (2024). Copyright 2024 Author(s) under CC BY 4.0 license, published by Springer Nature);[239] (c) monolithic wavelength beam-combined QCL array with integrated arrayed waveguide grating (Reproduced with permission from Karnik *et al*., Opt. Express **32**, 11681–11692 (2024). Copyright 2024 Optica Publishing Group);[248] (d) 15-to-5 channel wavelength multiplexer based on Rowland circle grating (Reproduced with permission from Gilles *et al*., Opt. Express **23**, 20288–20296 (2015). Copyright 2015 Optica Publishing Group);[249] (e) monolithic mid-infrared on-chip sensor composed by a QCL, a QCD, and a surface plasmon polariton waveguide (Reproduced under from Schwarz *et al*., Nat. Commun. **5**, 4085 (2014). Copyright 2014 Author(s) under CC BY-NC-SA 3.0 license, published by Springer Nature);[243] (f) buried InGaAs/InP integrated waveguides (Reproduced from Montesinos-Ballester *et al*., ACS Photonics **11**, 2236–2241 (2024). Copyright 2024 Author(s) under CC BY 4.0 license, published by American Chemical Society);[241] and (g) monolithic integration of QCL gain sections with passive InGaAs/InP waveguides through tapered sections (Reproduced with permission from Jung *et al*., Optica **6**, 1023–1030 (2019). Copyright 2019 Optica Publishing Group).[232]

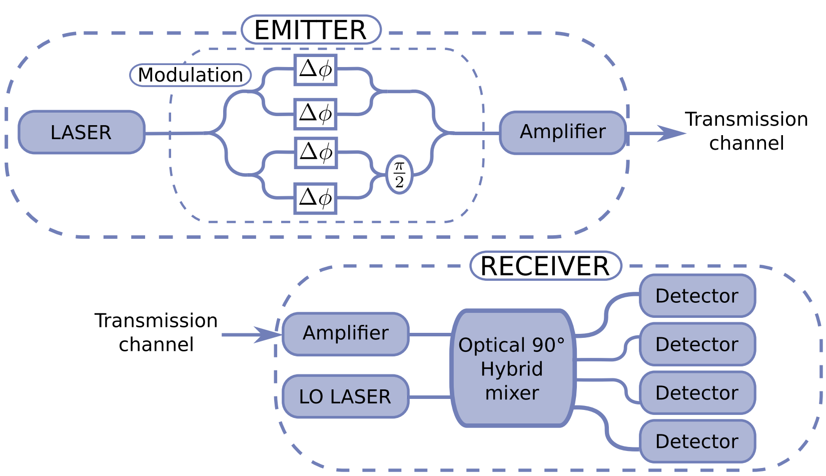

FIG. 16. Schematic representation of a typical QAM coherent transceiver architecture in photonic integrated circuits, using Mach–Zehnder modulators. Reproduced with permission from T. Poletti, "Optical phase and amplitude modulator and photonic integration for long wave infrared free space optical telecommunications," Ph.D. thesis, Université Paris Sciences et Lettres, 2024.[113]

The most direct way of doing that is to transmit the direct output of the laser and use it as a local oscillator (LO). The generated QAM signal is then coupled and transmitted into free space for communication purposes. During demodulation, differentiating between the two signals with different phases is crucial, and this requires transmitting an LO signal through free space as well. Due to uncertain power recovery of the LO signal in free space, another laser with a slightly shifted emission wavelength is used in the receiver. This laser is locked onto a detector, which detects the LO signal. By combining the LO beam with the QAM transmitted beam, a beating effect is created, allowing independent detection of the amplitude modulation associated with the two different phases, thereby enabling the demodulation process. Implementing a homodyne or heterodyne detection method would require two pairs of detectors with balanced detection, which is more complex and represented schematically in Fig. 16 but relaxes the constraint of transmitting the LO from the emitter laser, through the transmission channel.

In such coherent transceivers, the use of QCL and QCD is particularly advantageous due to their inherent high compatibility, as both are based on the same platform and technology, and especially to the passive nature and room temperature operation of the QCD. This simplifies their integration into the system. The QCD passive behavior eliminates the need for additional power sources, streamlining the overall design and integration process.

Phase modulation is an important concern for future developments, especially for transmission through turbulent media, such as the atmosphere. However, the currently available phase external modulators have limitations. Some have demonstrated high bandwidth but low phase-shift,[111] while others have unknown bandwidth with a limited 60° phase-shift,[112] or are in a more early stage of development in waveguide geometry.[113] Finally, it will be crucial to showcase the advantages of mid-infrared over near-infrared technologies in a real field environment. A comparative study over several hundred meters, directly comparing the near-infrared and mid-infrared wavelengths under challenging atmospheric conditions, should be performed. Adaptive optics will be essential for achieving precise pointing, turbulence compensation, and wavefront shaping, and the constraints imposed on them can be relaxed with the use of higher wavelengths.[251] The modeling of the propagation of a beam through a complex atmosphere (absorbing/diffusing medium), considering ballistic or snake photons, will be required as well as studying the degradation of the signal with conventional or chaos-encrypted modulation formats through fog.

C. FSO-to-RF

The THz domain is of prime interest for the spectroscopy of explosives and drugs,[252] for real-time imaging,[253] and for improving the capacity of free-space data communications.[254] For communication, the domain of interest lies approximately between 0.1 and 0.5 THz, which includes several atmospheric transparency bands.[255] A common method for generating a frequency carrier in this 0.1–0.5 THz band is to perform a heterodyne frequency beat with two ultra-stable, narrow-linewidth DFB lasers.[256] In this photonics-assisted THz transmission scheme, external modulation of one of the two lasers prior to the beating operation enables integration of the message to be transmitted.[257,258] Recent efforts have achieved data rates of hundreds of Gbits/s and converted heterodyne wave propagation over distances of more than 10 m.[259]

To date, this method has not been implemented with mid-infrared semiconductor lasers, as high-speed external modulators with large modulation depths are not yet widely available for these wavelengths. Conversely, the heterodyne beating of QCL DFBs in the mid-infrared has long been studied and used to characterize the bandwidth of mid-infrared detectors,[135] such as ultrafast QCDs and QWIPs. Indeed, typical frequency values for the direct modulation of QCLs[260,261] lag behind the peak bandwidths of QWIPs,[262] despite theoretical work showing a modulation bandwidth of QCLs of hundreds of GHz[263–265] due to their intersubband nature.[266] As mentioned above, the latest advances in unipolar quantum optoelectronics have enabled the development of Stark-effect modulators compatible with a wavelength of 9 μm (or in other words, a frequency of 33 THz).[176] The optimization and reduction in size of this new type of modulator should enable external modulation of a mid-infrared beam at frequencies up to 100 GHz and beyond. A monolithic platform for heterodyne transmitters and receivers can therefore facilitate a communication system that enables direct conversion of a signal transmitted by FSO into an RF signal. This conversion enables signals to be transmitted to end-users or applications requiring line-of-sight communication. Another application could also involve the use of a microwave photonics platform that incorporates two QCL DFBs, a QWIP and an external modulator for high-speed RF microwave generation. This configuration is of significant interest in the mid-infrared region due to the intersubband nature of the devices. The unique feature of these devices is their ability to handle high saturation currents while offering very high bandwidth potential, which is particularly interesting for this purpose. An initial demonstration was reported based on heterodyne beating of QCLs producing an RF carrier in the K_a band (between 26.5 and 40 GHz), which is of interest for 5G networks due to low atmospheric absorption.[267] As the bandwidth of QWIPs can be extended to hundreds of GHz, the unipolar heterodyne scheme of quantum optoelectronics should become a cost-effective method for generating waves in the 0.1–0.5 THz range and subsequently for performing photonics-assisted high-speed terahertz transmission.

VII. CONCLUSIONS

Free-space optical telecommunications represent a promising alternative to the gradual saturation of channels dedicated to wireless technologies and to growing bandwidth requirements. There is clearly a strong societal interest in proposing alternative solutions to counter atmospheric limitations and increase the range of optical telecommunications systems, even in degraded environments. The development of photonics technologies does have the potential to address secure and high-speed links, which can be combined with RF communication systems. In particular, recent advances in integrated MWIR and LWIR platforms will enable these communication systems to be developed further. Future performance will be boosted by the development of coherent communications, photonics integration, and WDM. The design of new components operating at mid-infrared wavelengths, such as modulators, ultrafast detectors, and even optical amplifiers,[268–270] will play an essential role in the growing development of such FSO communication systems. The refinement of filtering methods and the application of wavefront correction techniques to compensate for the effects of scattering and turbulence will also be necessary. Progress in the development of chalcogenide glass fibers for mid-infrared applications requiring the use of high-power lasers, chemical detection, thermal imaging, and temperature monitoring can also be beneficial for free-space optics applications. It is important to highlight the substantial potential of epitaxial ICLs for on-chip integrated technologies and in general of monolithic integration of mid-infrared devices into common photonic platforms.[271,272] Finally, let us quickly stress the importance of the progress of mid-infrared fiber lasers, which are mostly driven by high-quality fluoride glass fibers. Those sources have become the primary gain material for emissions up to 4 μm. Other mid-infrared transparent glasses, such as heavy metal oxides and chalcogenides, have faced challenges such as hydrogen diffusion, hence causing absorption issues and difficulties in achieving sufficient rare-earth doping. Despite this, recent advancements in precursor purification and fabrication techniques have led to successful mid-IR lasing beyond 5 μm. Therefore, we believe that mid-infrared fiber lasers are at present getting more mature although power and efficiency still need to be better improved especially beyond 4 μm emission wavelength. In addition, it will be very important to develop mid-infrared pulsed fiber lasers with high peak power and pulse energy.

In conclusion, this comprehensive paper demonstrates that the exciting developments of mid-infrared building blocks have opened new avenues in mid-infrared optoelectronics, extending beyond the realms of sensing and spectroscopy into the domain of free-space laser communications.

ACKNOWLEDGMENTS

The authors thank collaborators at Télécom Paris, Dr. Pierre Didier, Dr. Olivier Spitz, Huynah Kim, and Sara Zaminga. The authors specially thank Professor Carlo Sirtori from Ecole Normale Supérieure de Paris and Professor Laurent Cerutti from the University of Montpellier (France). We also acknowledge the financial support of mirSense, the Institut Mines-Télécom, The French National Agency of Research (ANR), the Direction Général de l'Armement (DGA), the Air Force Office for Scientific Research (AFSOR), and the European Union's Horizon 2020 Research and Innovation program.

AUTHOR DECLARATIONS

Conflict of Interest

The authors have no conflicts to disclose.

Author Contributions

All authors contributed equally.

Frédéric Grillot: Conceptualization (equal); Project administration (equal); Supervision (equal); Validation (equal); Writing – review & editing (equal). **Thomas Poletti**: Conceptualization (equal); Project administration (equal); Validation (equal); Writing – review & editing (equal). **Salvatore Pes**: Conceptualization (equal); Project administration (equal); Validation (equal); Writing – review & editing (equal).

DATA AVAILABILITY

The data that support the findings of this study are available from the corresponding author upon reasonable request.

REFERENCES

[1] A. Trichili, M. A. Cox, B. S. Ooi, and M.-S. Alouini, "Roadmap to free space optics," J. Opt. Soc. Am. B **37**, A184 (2020).

[2] I. Gordon, L. Rothman, R. Hargreaves, R. Hashemi, E. Karlovets, F. Skinner, E. Conway, C. Hill, R. Kochanov, Y. Tan, P. Wcisło, A. Finenko, K. Nelson, P. Bernath, M. Birk, V. Boudon, A. Campargue, K. Chance, A. Coustenis, B. Drouin, J. Flaud, R. Gamache, J. Hodges, D. Jacquemart, E. Mlawer, A. Nikitin, V. Perevalov, M. Rotger, J. Tennyson, G. Toon, H. Tran, V. Tyuterev, E. Adkins, A. Baker, A. Barbe, E. Canè, A. Császár, A. Dudaryonok, O. Egorov, A. Fleisher, H. Fleurbaey, A. Foltynowicz, T. Furtenbacher, J. Harrison, J. Hartmann, V. Horneman, X. Huang, T. Karman, J. Karns, S. Kassi, I. Kleiner, V. Kofman, F. KwabiaTchana-, N. Lavrentieva, T. Lee, D. Long, A. Lukashevskaya, O. Lyulin, V. Makhnev, W. Matt, S. Massie, M. Melosso, S. Mikhailenko, D. Mondelain, H. Müller, O. Naumenko, A. Perrin, O. Polyansky, E. Raddaoui, P. Raston, Z. Reed, M. Rey, C. Richard, R. Tóbiás, I. Sadiek, D. Schwenke, E. Starikova, K. Sung, F. Tamassia, S. Tashkun, J. Vander Auwera, I. Vasilenko, A. Vigasin, G. Villanueva, B. Vispoel, G. Wagner, A. Yachmenev, and S. Yurchenko, "The HITRAN2020 molecular spectroscopic database," J. Quant. Spectrosc. Radiat. Transfer **277**, 107949 (2022).

[3] Y. Horst, B. I. Bitachon, L. Kulmer, J. Brun, T. Blatter, J.-M. Conan, A. Montmerle-Bonnefois, J. Montri, B. Sorrente, C. B. Lim, N. Védrenne, D. Matter, L. Pommarel, B. Baeuerle, and J. Leuthold, "Tbit/s line-rate satellite feeder links enabled by coherent modulation and full-adaptive optics," Light: Sci. Appl. **12**, 153 (2023).

[4] Commercialized FSO system, https://www.caci.com/optical-and-photonic-solutions (2023); accessed 17 July 2023.

[5] TereScope 10GE, the industry's first wireless 10 gigabit ethernet free space optics system, https://commconnect.com/wp-content/uploads/2011/10/terescope-10ge.pdf (2023).

[6] J. Wang, S. Li, M. Luo, J. Liu, L. Zhu, C. Li, D. Xie, Q. Yang, S. Yu, J. Sun *et al.*, "N-dimensional multiplexing link with 1.036-Pbit/s transmission capacity and 112.6-bit/s/Hz spectral efficiency using OFDM-8QAM signals over 368 WDM pol-muxed 26 OAM modes," in *2014 The European Conference on Optical Communication (ECOC)* (IEEE, 2014), pp. 1–3.

[7] J. Faist, F. Capasso, D. L. Sivco, C. Sirtori, A. L. Hutchinson, and A. Y. Cho, "Quantum cascade laser," Science **264**, 553–556 (1994).

[8] F. Capasso, K. Mohammed, and A. Y. Cho, "Sequential resonant tunneling through a multiquantum well superlattice," Appl. Phys. Lett. **48**, 478–480 (1986).

[9] J. S. Roberts, R. P. Green, L. R. Wilson, E. A. Zibik, D. G. Revin, J. W. Cockburn, and R. J. Airey, "Quantum cascade lasers grown by metalorganic vapor phase epitaxy," Appl. Phys. Lett. **82**, 4221–4223 (2003).

[10] C. Gmachl, F. Capasso, D. L. Sivco, and A. Y. Cho, "Recent progress in quantum cascade lasers and applications," Rep. Prog. Phys. **64**, 1533 (2001).

[11] J. Faist, F. Capasso, C. Sirtori, D. L. Sivco, J. N. Baillargeon, A. L. Hutchinson, S.-N. G. Chu, and A. Y. Cho, "High power mid-infrared ($\lambda \sim 5$ μm) quantum cascade lasers operating above room temperature," Appl. Phys. Lett. **68**, 3680–3682 (1996).

[12] S. Blaser, D. A. Yarekha, L. Hvozdara, Y. Bonetti, A. Muller, M. Giovannini, and J. Faist, "Room-temperature, continuous-wave, single-mode quantum-cascade lasers at $\lambda \simeq 5.4$ μm," Appl. Phys. Lett. **86**, 041109 (2005).

[13] M. Troccoli, S. Corzine, D. Bour, J. Zhu, O. Assayag, L. Diehl, B. Lee, G. Höfler, and F. Capasso, "Room temperature continuous-wave operation of quantum-cascade lasers grown by metal organic vapour phase epitaxy," Electron. Lett. **41**, 1059 (2005).

[14] A. Hugi, G. Villares, S. Blaser, H. Liu, and J. Faist, "Mid-infrared frequency comb based on a quantum cascade laser," Nature **492**, 229–233 (2012).

[15] G. Villares, A. Hugi, S. Blaser, and J. Faist, "Dual-comb spectroscopy based on quantum-cascade-laser frequency combs," Nat. Commun. **5**, 5192 (2014).

[16] I. Coddington, N. Newbury, and W. Swann, "Dual-comb spectroscopy," Optica **3**, 414–426 (2016).

[17] H. Wright, J. Sun, D. McKendrick, N. Weston, and D. T. Reid, "Two-photon dual-comb LiDAR," Opt. Express **29**, 37037–37047 (2021).

[18] I. Heckelmann, M. Bertrand, A. Dikopoltsev, M. Beck, G. Scalari, and J. Faist, "Quantum walk comb in a fast gain laser," Science **382**, 434–438 (2023).

[19] Y. Bai, N. Bandyopadhyay, S. Tsao, S. Slivken, and M. Razeghi, "Room temperature quantum cascade lasers with 27% wall plug efficiency," Appl. Phys. Lett. **98**, 181102 (2011).

[20] S. Slivken and M. Razeghi, "High power mid-infrared quantum cascade lasers grown on GaAs," Photonics **9**(4), 231 (2022).

[21] F. Wang, S. Slivken, D. Wu, and M. Razeghi, "Room temperature quantum cascade lasers with 22% wall plug efficiency in continuous-wave operation," Opt. Express **28**, 17532–17538 (2020).

[22] R. Yang, "Interband cascade lasers target the mid-infrared," Compd. Semicond. **25**, 48–53 (2019).

[23] Q. Y. Lu, Y. Bai, N. Bandyopadhyay, S. Slivken, and M. Razeghi, "2.4 W room temperature continuous wave operation of distributed feedback quantum cascade lasers," Appl. Phys. Lett. **98**, 181106 (2011).

[24] J. Faist, C. Gmachl, F. Capasso, C. Sirtori, D. L. Sivco, J. N. Baillargeon, and A. Y. Cho, "Distributed feedback quantum cascade lasers," Appl. Phys. Lett. **70**, 2670–2672 (1997).

[25]L. Bizet, R. Vallon, B. Parvitte, M. Brun, G. Maisons, M. Carras, and V. Zeninari, "Multi-gas sensing with quantum cascade laser array in the mid-infrared region," Appl. Phys. B **123**, 145 (2017).
[26]V. Zéninari, R. Vallon, L. Bizet, C. Jacquemin, G. Aoust, G. Maisons, M. Carras, and B. Parvitte, "Widely-tunable quantum cascade-based sources for the development of optical gas sensors," Sensors **20**, 6650 (2020).
[27]Y.-J. Guan, X.-F. Jia, S.-S. Li, L.-J. Wang, N. Zhuo, J.-C. Zhang, S.-Q. Zhai, J.-Q. Liu, S.-M. Liu, F.-Q. Liu, and Z. G. Wang, "High power tapered sampling grating distributed feedback quantum cascade lasers," IEEE Photonics Technol. Lett. **32**, 305–308 (2020).
[28]H. Nguyen Van, Z. Loghmari, H. Philip, M. Bahriz, A. N. Baranov, and R. Teissier,"Long wavelength (λ > 17 μm) distributed feedback quantum cascade lasers operating in a continuous wave at room temperature," Photonics **6**(1), 31 (2019).
[29]B. Hinkov, F. Pilat, L. Lux, P. L. Souza, M. David, A. Schwaighofer, D. Ristanić, B. Schwarz, H. Detz, A. M. Andrews *et al.*, "A mid-infrared lab-on-a-chip for dynamic reaction monitoring," Nat. Commun. **13**, 4753 (2022).
[30]R. Köhler, A. Tredicucci, F. Beltram, H. E. Beere, E. H. Linfield, A. G. Davies, D. A. Ritchie, R. C. Iotti, and F. Rossi, "Terahertz semiconductor-heterostructure laser," Nature **417**, 156–159 (2002).
[31]B. S. Williams, "Terahertz quantum-cascade lasers," Nat. Photonics **1**, 517–525 (2007).
[32]B. S. Williams, S. Kumar, Q. Hu, and J. L. Reno, "Operation of terahertz quantum-cascade lasers at 164 K in pulsed mode and at 117 K in continuous-wave mode," Opt. Express **13**, 3331–3339 (2005).
[33]L. Bosco, M. Franckié, G. Scalari, M. Beck, A. Wacker, and J. Faist, "Thermoelectrically cooled THz quantum cascade laser operating up to 210 K," Appl. Phys. Lett. **115**, 010601 (2019).
[34]A. Khalatpour, A. K. Paulsen, C. Deimert, Z. R. Wasilewski, and Q. Hu, "High-power portable terahertz laser systems," Nat. Photonics **15**, 16–20 (2021).
[35]A. Wade, G. Fedorov, D. Smirnov, S. Kumar, B. Williams, Q. Hu, and J. Reno, "Magnetic-field-assisted terahertz quantum cascade laser operating up to 225 K," Nat. Photonics **3**, 41–45 (2009).
[36]K. Fujita, S. Jung, Y. Jiang, J. H. Kim, A. Nakanishi, A. Ito, M. Hitaka, T. Edamura, and M. A. Belkin, "Recent progress in terahertz difference-frequency quantum cascade laser sources," Nanophotonics **7**, 1795–1817 (2018).
[37]J. Meyer, C. Hoffman, F. Bartoli, and L. Ram-Mohan, "Type-II quantum-well lasers for the mid-wavelength infrared," Appl. Phys. Lett. **67**, 757–759 (1995).
[38]I. Vurgaftman, R. Weih, M. Kamp, J. Meyer, C. Canedy, C. Kim, M. Kim, W. Bewley, C. Merritt, J. Abell, and S. Höfling, "Interband cascade lasers," J. Phys. D: Appl. Phys. **48**, 123001 (2015).
[39]P. Didier, O. Spitz, L. Cerutti, D. Diaz-Thomas, A. Baranov, M. Carras, and F. Grillot, "Relative intensity noise and intrinsic properties of RF mounted interband cascade laser," Appl. Phys. Lett. **119**, 171107 (2021).
[40]See https://microdevices.jpl.nasa.gov/capabilities/in-situ-instruments-tls/tls-mars/ for "Lasers on Mars keep going" (NASA, 2023); accessed 07 July 2023.
[41]C.-H. Lin, R. Q. Yang, D. Zhang, S. Murry, S. Pei, A. Allerman, and S. Kurtz, "Type-II interband quantum cascade laser at 3.8 µm," Electron. Lett. **33**, 598 (1997).
[42]R. Yang, J. Bruno, J. Bradshaw, J. Pham, and D. Wortman, "High-power interband cascade lasers with quantum efficiency > 450%," Electron. Lett. **35**, 1254–1255 (1999).
[43]R. Q. Yang, J. Bruno, J. Bradshaw, J. Pham, and D. Wortman, "Interband cascade lasers: Progress and challenges," Physica E **7**, 69–75 (2000).
[44]R. Q. Yang, J. L. Bradshaw, J. Bruno, J. Pham, and D. Wortman, "Power, efficiency, and thermal characteristics of type-II interband cascade lasers," IEEE J. Quantum Electron. **37**, 282–289 (2001).
[45]J. L. Bradshaw, J. Pham, R. Q. Yang, J. Bruno, and D. Wortman, "Enhanced CW performance of the interband cascade laser using improved device fabrication," IEEE J. Sel. Top. Quantum Electron. **7**, 102–105 (2001).
[46]R. Q. Yang, J. Bradshaw, J. Bruno, J. Pham, and D. Wortman, "Mid-infrared type-II interband cascade lasers," IEEE J. Quantum Electron. **38**, 559–568 (2002).
[47]M. Kim, C. Canedy, W. Bewley, C. Kim, J. Lindle, J. Abell, I. Vurgaftman, and J. Meyer, "Interband cascade laser emitting at λ = 3.75 μm in continuous wave above room temperature," Appl. Phys. Lett. **92**, 191110 (2008).
[48]I. Vurgaftman, W. W. Bewley, C. L. Canedy, C. S. Kim, M. Kim, C. D. Merritt, J. Abell, and J. R. Meyer, "Interband cascade lasers with low threshold powers and high output powers," IEEE J. Sel. Top. Quantum Electron. **19**, 1200210 (2013).
[49]C. L. Canedy, J. Abell, C. D. Merritt, W. W. Bewley, C. S. Kim, M. Kim, I. Vurgaftman, and J. R. Meyer, "Pulsed and CW performance of 7-stage interband cascade lasers," Opt. Express **22**, 7702–7710 (2014).
[50]I. Vurgaftman, W. Bewley, C. Canedy, C. Kim, M. Kim, C. Merritt, J. Abell, J. Lindle, and J. Meyer, "Rebalancing of internally generated carriers for mid-infrared interband cascade lasers with very low power consumption," Nat. Commun. **2**, 585 (2011).
[51]A. Spott, E. J. Stanton, A. Torres, M. L. Davenport, C. L. Canedy, I. Vurgaftman, M. Kim, C. S. Kim, C. D. Merritt, W. W. Bewley *et al.*, "Interband cascade laser on silicon," Optica **5**, 996–1005 (2018).
[52]L. Cerutti, D. A. Díaz Thomas, J.-B. Rodriguez, M. Rio Calvo, G. Patriarche, A. N. Baranov, and E. Tournié, "Quantum well interband semiconductor lasers highly tolerant to dislocations," Optica **8**, 1397–1402 (2021).
[53]S. Zaminga, P. Didier, H. Kim, D. A. Díaz-Thomas, A. N. Baranov, J. B. Rodriguez, E. Tournié, H. Knötig, O. Spitz, B. Schwarz, L. Cerutti, and F. Grillot, "Free-space gigabit data transmission with a directly modulated interband cascade laser epitaxially grown on silicon," in *2023 IEEE Photonics Conference (IPC)* (IEEE, 2023), pp. 1–2.
[54]R. Soref, "Mid-infrared photonics in silicon and germanium," Nat. Photonics **4**, 495–497 (2010).
[55]D. Liang and J. E. Bowers, "Recent progress in lasers on silicon," Nat. Photonics **4**, 511–517 (2010).
[56]Y. Matsuoka, M. P. Semtsiv, and W. T. Masselink, "Quantum cascade lasers," in *Mid-Infrared Optoelectronics, Woodhead Publishing Series in Electronic and Optical Materials*, edited by E. Tournié and L. Cerutti (Woodhead Publishing, 2020), Chap. 4, pp. 131–179.
[57]L. Cerutti, A. Vicet, and E. Tournié, "Interband mid-infrared lasers," in *Mid-Infrared Optoelectronics, Woodhead Publishing Series in Electronic and Optical Materials*, edited by E. Tournié and L. Cerutti (Woodhead Publishing, 2020), Chap. 3, pp. 91–130.
[58]J. A. Massengale, Y. Shen, R. Q. Yang, S. D. Hawkins, and J. F. Klem, "Long wavelength interband cascade lasers," Appl. Phys. Lett. **120**, 091105 (2022).
[59]Y. Shen, R. Q. Yang, S. D. Hawkins, and A. J. Muhowski, "Continuous wave interband cascade lasers near 13 μm," J. Vac. Sci. Technol. B **42**, 022206 (2024).
[60]R. Weih, L. Nahle, S. Hofling, J. Koeth, and M. Kamp, "Single mode interband cascade lasers based on lateral metal gratings," Appl. Phys. Lett. **105**, 071111 (2014).
[61]C. Merritt, W. Bewley, C. Canedy, C. S. Kim, M. Kim, M. Warren, I. Vurgaftman, and J. Meyer, "Distributed feedback interband cascade lasers with reduced contact duty cycles," Proc. SPIE **9855** 98550C (2016).
[62]C. S. Kim, M. Kim, J. Abell, W. W. Bewley, C. D. Merritt, C. L. Canedy, I. Vurgaftman, and J. R. Meyer, "Mid-infrared distributed-feedback interband cascade lasers with continuous-wave single-mode emission to 80 °C," Appl. Phys. Lett. **101**, 061104 (2012).
[63]J. Fordyce, D. Diaz-Thomas, L. O'Faolain, A. Baranov, T. Piwonski, and L. Cerutti, "Single-mode interband cascade laser with a slotted waveguide," Appl. Phys. Lett. **121**, 211102 (2022).
[64]M. von Edlinger, R. Weih, J. Scheuermann, L. Nahle, M. Fischer, J. Koeth, M. Kamp, and S. Höfling, "Monolithic single mode interband cascade lasers with wide wavelength tunability," Appl. Phys. Lett. **109**, 201109 (2016).
[65]E. Giraud, P. Demolon, T. Gresch, L. Urio, A. Muller, and R. Maulini, "Room-temperature continuous-wave external cavity interband cascade laser tunable from 3.2 to 3.6 μm," Opt. Express **29**, 38291–38297 (2021).
[66]J. Gong, R. Q. Yang, Z. Wang, and J.-J. He, "Single-mode tunable interband cascade laser emitting at 3.4 μm with a wide tuning range over 100 nm," IEEE Photonics Technol. Lett. **35**, 309–312 (2023).
[67]J. R. Meyer, W. W. Bewley, C. L. Canedy, C. S. Kim, M. Kim, C. D. Merritt, and I. Vurgaftman, "The interband cascade laser," Photonics **7**, 75 (2020).
[68]J. Faist, "Wallplug efficiency of quantum cascade lasers: Critical parameters and fundamental limits," Appl. Phys. Lett. **90**, 253512 (2007).
[69]N. Mustafa, L. Pesquera, C. Cheung, and K. Shore, "Terahertz bandwidth prediction for amplitude modulation response of unipolar intersubband semiconductor lasers," IEEE Photonics Technol. Lett. **11**, 527–529 (1999).

[70] W. Bewley, J. Lindle, C. Kim, M. Kim, C. Canedy, I. Vurgaftman, and J. Meyer, "Lifetimes and Auger coefficients in type-II W interband cascade lasers," Appl. Phys. Lett. **93**, 041118 (2008).
[71] H. Y. Fan, "Effects of free carriers on the optical properties," in *Semiconductors and Semimetals* (Elsevier, 1967), pp. 405–419.
[72] M. A. Van Camp, S. Assefa, D. M. Gill, T. Barwicz, S. M. Shank, P. M. Rice, T. Topuria, and W. M. J. Green, "Demonstration of electrooptic modulation at 2165 nm using a silicon Mach-Zehnder interferometer," Opt. Express **20**, 28009–28016 (2012).
[73] W. Cao, S. Liu, C. G. Littlejohns, D. J. Thomson, M. Nedeljkovic, W. Zhang, K. Li, M. Banakar, Y. Tran, X. Yan, H. Du, Z. Ren, F. Gardes, G. T. Reed, and G. Z. Mashanovich, "High-speed silicon Michelson interferometer modulator and streamlined IMDD PAM-4 transmission of Mach-Zehnder modulators for the 2 μm wavelength band," Opt. Express **29**, 14438–14451 (2021).
[74] M. Nedeljkovic, C. G. Littlejohns, A. Z. Khokhar, M. Banakar, W. Cao, J. S. Penades, D. T. Tran, F. Y. Gardes, D. J. Thomson, G. T. Reed, H. Wang, and G. Z. Mashanovich, "Silicon-on-insulator free-carrier injection modulators for the mid-infrared," Opt. Lett. **44**, 915 (2019).
[75] M. Montesinos-Ballester, V. Vakarin, J. M. Ramirez, Q. Liu, C. Alonso-Ramos, X. Le Roux, J. Frigerio, A. Ballabio, A. Barzaghi, L. Deniel, D. Bouville, L. Vivien, G. Isella, and D. Marris-Morini, "Optical modulation in Ge-rich SiGe waveguides in the mid-infrared wavelength range up to 11 μm," Commun. Mater. **1**, 6 (2020).
[76] W. Cao, D. Hagan, D. J. Thomson, M. Nedeljkovic, C. G. Littlejohns, A. Knights, S.-U. Alam, J. Wang, F. Gardes, W. Zhang, S. Liu, K. Li, M. S. Rouifed, G. Xin, W. Wang, H. Wang, G. T. Reed, and G. Z. Mashanovich, "High-speed silicon modulators for the 2 μm wavelength band," Optica **5**, 1055 (2018).
[77] X. Wang, W. Shen, W. Li, Y. Liu, Y. Yao, J. Du, Q. Song, and K. Xu, "High-speed silicon photonic Mach–Zehnder modulator at 2 μm," Photonics Res. **9**, 535 (2021).
[78] J. Kang, M. Takenaka, and S. Takagi, "Novel Ge waveguide platform on Ge-on-insulator wafer for mid-infrared photonic integrated circuits," Opt. Express **24**, 11855 (2016).
[79] R. A. Soref, S. J. Emelett, and W. R. Buchwald, "Silicon waveguided components for the long-wave infrared region," J. Opt. A: Pure Appl. Opt. **8**, 840–848 (2006).
[80] D. Ren, C. Dong, and D. Burghoff, "Integrated nonlinear photonics in the longwave-infrared: A roadmap," MRS Commun. **13**, 942–956 (2023).
[81] T. Li, M. Nedeljkovic, N. Hattasan, W. Cao, Z. Qu, C. G. Littlejohns, J. S. Penades, L. Mastronardi, V. Mittal, D. Benedikovic, D. J. Thomson, F. Y. Gardes, H. Wu, Z. Zhou, and G. Z. Mashanovich, "Ge-on-Si modulators operating at mid-infrared wavelengths up to 8 μm," Photonics Res. **7**, 828 (2019).
[82] M. Montesinos-Ballester, L. Deniel, N. Koompai, T. H. N. Nguyen, J. Frigerio, A. Ballabio, V. Falcone, X. Le Roux, C. Alonso-Ramos, L. Vivien, A. Bousseksou, G. Isella, and D. Marris-Morini, "Mid-infrared integrated electro-optic modulator operating up to 225 MHz between 6.4 and 10.7 μm wavelength," ACS Photonics **9**, 249–255 (2022).
[83] T. H. N. Nguyen, N. Koompai, V. Turpaud, M. Montesinos-Ballester, J. Peltier, J. Frigerio, A. Ballabio, R. Giani, J.-R. Coudevylle, C. Villebasse, D. Bouville, C. Alonso-Ramos, L. Vivien, G. Isella, and D. Marris-Morini, "1 GHz electro-optical silicon-germanium modulator in the 5-9 μm wavelength range," Opt. Express **30**, 47093–47102 (2022).
[84] T. H. N. Nguyen, V. Turpaud, N. Koompai, J. Peltier, S. Calcaterra, G. Isella, J.-R. Coudevylle, C. Alonso-Ramos, L. Vivien, J. Frigerio, and D. Marris-Morini, "Integrated PIN modulator and photodetector operating in the mid-infrared range from 5.5 μm to 10 μm," Nanophotonics **13**, 1803–1813 (2024).
[85] J. Chiles and S. Fathpour, "Mid-infrared integrated waveguide modulators based on silicon-on-lithium-niobate photonics," Optica **1**, 350 (2014).
[86] M. Li, J. Ling, Y. He, U. A. Javid, S. Xue, and Q. Lin, "Lithium niobate photonic-crystal electro-optic modulator," Nat. Commun. **11**, 4123 (2020).
[87] A. Melikyan, L. Alloatti, A. Muslija, D. Hillerkuss, P. C. Schindler, J. Li, R. Palmer, D. Korn, S. Muehlbrandt, D. Van Thourhout, B. Chen, R. Dinu, M. Sommer, C. Koos, M. Kohl, W. Freude, and J. Leuthold, "High-speed plasmonic phase modulators," Nat. Photonics **8**, 229–233 (2014).
[88] S. Zhu, G. Q. Lo, and D. L. Kwong, "Phase modulation in horizontal metal-insulator-silicon-insulator-metal plasmonic waveguides," Opt. Express **21**, 8320–8330 (2013).
[89] Y. Hinakura, H. Arai, and T. Baba, "64 Gbps Si photonic crystal slow light modulator by electro-optic phase matching," Opt. Express **27**, 14321–14327 (2019).
[90] T. Xu, Y. Dong, Q. Zhong, S. Zheng, Y. Qiu, X. Zhao, L. Jia, C. Lee, and T. Hu, "Mid-infrared integrated electro-optic modulators: A review," Nanophotonics **12**, 3683–3706 (2023).
[91] L. Duvillaret, S. Rialland, and J.-L. Coutaz, "Electro-optic sensors for electric field measurements II choice of the crystals and complete optimization of their orientation," J. Opt. Soc. Am. B **19**, 2704 (2002).
[92] G. Gaborit, J. Dahdah, F. Lecoche, P. Jarrige, Y. Gaeremynck, E. Duraz, and L. Duvillaret, "A nonperturbative electrooptic sensor for in situ electric discharge characterization," IEEE Trans. Plasma Sci. **41**, 2851–2857 (2013).
[93] J. Nag, J. D. Ryckman, S. M. Weiss, and R. F. Haglund, "Silicon photonics with active (phase change) materials for optical modulators," in *Encyclopedia of Materials: Electronics* (Elsevier, 2023), pp. 334–352.
[94] B. Pan, J. Hu, Y. Huang, L. Song, J. Wang, P. Chen, Z. Yu, L. Liu, and D. Dai, "Demonstration of high-speed thin-film lithium-niobate-on-insulator optical modulators at the 2-μm wavelength," Opt. Express **29**, 17710–17717 (2021).
[95] T. Jin, J. Zhou, and P. T. Lin, "Mid-Infrared electro-optical modulation using monolithically integrated titanium dioxide on lithium niobate optical waveguides," Sci. Rep. **9**, 15130 (2019).
[96] J. Liu, G. Xu, F. Liu, I. Kityk, X. Liu, and Z. Zhen, "Recent advances in polymer electro-optic modulators," RSC Adv. **5**, 15784–15794 (2015).
[97] A. Cingolani, M. Ferrara, M. Lugarà, and F. Lévy, "Pockels effect in gallium selenide," Solid State Commun. **29**, 677–679 (1979).
[98] D. A. B. Miller, D. S. Chemla, T. C. Damen, A. C. Gossard, W. Wiegmann, T. H. Wood, and C. A. Burrus, "Band-edge electroabsorption in quantum well structures: The quantum-confined Stark effect," Phys. Rev. Lett. **53**, 2173–2176 (1984).
[99] D. A. Miller, D. S. Chemla, T. C. Damen, A. C. Gossard, W. Wiegmann, T. H. Wood, and C. A. Burrus, "Electric field dependence of optical absorption near the band gap of quantum-well structures," Phys. Rev. B **32**, 1043–1060 (1985).
[100] *Fibre Optic Communication*, 2nd ed., *Springer Series in Optical Sciences*, edited by H. Venghaus and N. Grote (Springer International Publishing, Cham, Switzerland, 2017).
[101] Y.-H. Kuo, Y. K. Lee, Y. Ge, S. Ren, J. E. Roth, T. I. Kamins, D. A. B. Miller, and J. S. Harris, "Strong quantum-confined Stark effect in germanium quantum-well structures on silicon," Nature **437**, 1334–1336 (2005).
[102] J. Frigerio, V. Vakarin, P. Chaisakul, M. Ferretto, D. Chrastina, X. Le Roux, L. Vivien, G. Isella, and D. Marris-Morini, "Giant electro-optic effect in Ge/SiGe coupled quantum wells," Sci. Rep. **5**, 15398 (2015).
[103] R. P. G. Karunasiri, Y. J. Mii, and K. L. Wang, "Tunable infrared modulator and switch using Stark shift in step quantum wells," IEEE Electron Device Lett. **11**, 227–229 (1990).
[104] E. Dupont, D. Delacourt, V. Berger, N. Vodjdani, and M. Papuchon, "Phase and amplitude modulation based on intersubband transitions in electron transfer double quantum wells," Appl. Phys. Lett. **62**, 1907–1909 (1993).
[105] E. B. Dupont, D. Delacourt, and M. Papuchon, "Mid-infrared phase modulation via Stark effect on intersubband transitions in GaAs/GaAlAs quantum wells," IEEE J. Quantum Electron. **29**, 2313–2318 (1993).
[106] P. F. Yuh and K. L. Wang, "Large Stark effects for transitions from local states to global states in quantum well structures," IEEE J. Quantum Electron. **25**, 1671–1676 (1989).
[107] N. Vodjdani, B. Vinter, V. Berger, E. Böckenhoff, and E. Costard, "Tunneling assisted modulation of the intersubband absorption in double quantum wells," Appl. Phys. Lett. **59**, 555–557 (1991).
[108] C. Sirtori, F. Capasso, D. L. Sivco, A. L. Hutchinson, and A. Y. Cho, "Resonant Stark tuning of second-order susceptibility in coupled quantum wells," Appl. Phys. Lett. **60**, 151–153 (1992).
[109] J. Teissier, S. Laurent, C. Manquest, C. Sirtori, A. Bousseksou, J. R. Coudevylle, R. Colombelli, G. Beaudoin, and I. Sagnes, "Electrical modulation of the complex refractive index in mid-infrared quantum cascade lasers," Opt. Express **20**, 1172–1183 (2012).
[110] P. Didier, H. Dely, T. Bonazzi, O. Spitz, E. Awwad, E. Rodriguez, A. Vasanelli, C. Sirtori, and F. Grillot, "High-capacity free-space optical link in the midinfrared

thermal atmospheric windows using unipolar quantum devices," Adv. Photonics **4**, 056004 (2022).
[111] H. Dely, B. Chomet, T. Bonazzi, D. Gacemi, A. Vasanelli, A. Evirgen, O. Lopez, B. Darquié, F. Kapsalidis, J. Faist, and C. Sirtori, "Heterodyne coherent detection of phase modulation in a mid-infrared unipolar device," Opt. Express **31**, 30876–30883 (2023).
[112] H. Chung, I. Hwang, J. Yu, G. Boehm, M. A. Belkin, and J. Lee, "Electrical phase modulation based on mid-infrared intersubband polaritonic metasurfaces," Adv. Sci. **10**, 2207520 (2023).
[113] T. Poletti, "Optical phase and amplitude modulator and photonic integration for long wave infrared free space optical telecommunications," Ph.D. thesis, Université Paris Sciences et Lettres, 2024.
[114] A. Barzaghi, V. Falcone, S. Calcaterra, D. Marris-Morini, M. Virgilio, and J. Frigerio, "Modelling of an intersubband quantum confined Stark effect in Ge quantum wells for mid-infrared photonics," Opt. Express **30**, 46710–46721 (2022).
[115] H. Lin, Y. Song, Y. Huang, D. Kita, S. Deckoff-Jones, K. Wang, L. Li, J. Li, H. Zheng, Z. Luo, H. Wang, S. Novak, A. Yadav, C.-C. Huang, R.-J. Shiue, D. Englund, T. Gu, D. Hewak, K. Richardson, J. Kong, and J. Hu, "Chalcogenide glass-on-graphene photonics," Nat. Photonics **11**, 798–805 (2017).
[116] S. Pirotta, N.-L. Tran, A. Jollivet, G. Biasiol, P. Crozat, J.-M. Manceau, A. Bousseksou, and R. Colombelli, "Fast amplitude modulation up to 1.5 GHz of mid-IR free-space beams at room-temperature," Nat. Commun. **12**, 799 (2021).
[117] M. Malerba, S. Pirotta, G. Aubin, L. Lucia, M. Jeannin, J.-M. Manceau, A. Bousseksou, Q. Lin, J.-F. Lampin, E. Peytavit, S. Barbieri, L. H. Li, A. G. Davies, E. H. Linfield, and R. Colombelli, "Ultrafast (≈10 GHz) mid-IR modulator based on ultrafast electrical switching of the light–matter coupling," Appl. Phys. Lett. **125**, 041101 (2024).
[118] A. E.-S. Abd-Elkader, B. M. Younis, M. F. O. Hameed, and S. S. A. Obayya, "Polarization independent silicon on calcium fluoride-based MIR optical modulator," Opt. Quantum Electron. **55**, 378 (2023).
[119] W. Lawson, S. Nielsen, E. Putley, and A. Young, "Preparation and properties of HgTe and mixed crystals of HgTe-CdTe," J. Phys. Chem. Solids **9**, 325–329 (1959).
[120] B. Bartlett, D. Charlton, W. Dunn, P. Ellen, M. Jenner, and M. Jervis, "Background limited photoconductive HgCdTe detectors for use in the 8–14 micron atmospheric window," Infrared Phys. **9**, 35–36 (1969).
[121] A. Singh, A. Shukla, and R. Pal, "High performance of midwave infrared HgCdTe e-avalanche photodiode detector," IEEE Electron Device Lett. **36**, 360–362 (2015).
[122] M. Kopytko, A. Kębłowski, W. Gawron, P. Madejczyk, A. Kowalewski, and K. Jóźwikowski, "High-operating temperature MWIR nBn HgCdTe detector grown by MOCVD," Opto-Electron. Rev. **21**, 402–405 (2013).
[123] P. Guyot-Sionnest and J. A. Roberts, "Background limited mid-infrared photodetection with photovoltaic HgTe colloidal quantum dots," Appl. Phys. Lett. **107**, 253104 (2015).
[124] 1 GHz 3 dB-bandwidth MCT detector, https://vigophotonics.com/product/fip-series/ (2023); accessed 31 May 2023.
[125] K.-K. Choi, B. Levine, C. Bethea, J. Walker, and R. Malik, "Multiple quantum well 10 μm $GaAs/Al_xGa_{1-x}$ as infrared detector with improved responsivity," Appl. Phys. Lett. **50**, 1814–1816 (1987).
[126] B. Levine, "Quantum-well infrared photodetectors," J. Appl. Phys. **74**, R1–R81 (1993).
[127] Q. Lin, M. Hakl, S. Lepillet, H. Li, J.-F. Lampin, E. Peytavit, and S. Barbieri, "Real-time, chirped-pulse heterodyne detection at room temperature with 100 GHz 3-dB-bandwidth mid-infrared quantum-well photodetectors," Optica **10**, 1700–1708 (2023).
[128] P. Grant, R. Dudek, L. Wolfson, M. Buchanan, and H. Liu, "Ultra-high frequency monolithically integrated quantum well infrared photodetector up to 75 GHz," Electron. Lett. **41**, 214–215 (2005).
[129] W. A. Beck and M. S. Mirotznik, "Microstrip antenna coupling for quantum-well infrared photodetectors," Infrared Phys. Technol. **42**, 189–198 (2001).
[130] D. Palaferri, Y. Todorov, A. Bigioli, A. Mottaghizadeh, D. Gacemi, A. Calabrese, A. Vasanelli, L. Li, A. G. Davies, E. H. Linfield, F. Kapsalidis, M. Beck, J. Faist, and C. Sirtori, "Room-temperature nine-μm-wavelength photodetectors and GHz-frequency heterodyne receivers," Nature **556**, 85–88 (2018).
[131] M. Hakl, Q. Lin, S. Lepillet, M. Billet, J.-F. Lampin, S. Pirotta, R. Colombelli, W. Wan, J. Cao, H. Li *et al.*, "Ultrafast quantum-well photodetectors operating at 10 μm with a flat frequency response up to 70 GHz at room temperature," ACS Photonics **8**, 464–471 (2021).
[132] Q. Lin, M. Hakl, J.-F. Lampin, W. Wan, J. Cao, H. Li, E. Peytavit, and S. Barbieri, "Frequency response of patch-array QWIP photodetectors up to 220 GHz via mid-infrared photomixing," Proc. SPIE **PC12430**, PC124300R (2023).
[133] D. Hofstetter, M. Beck, and J. Faist, "Quantum-cascade-laser structures as photodetectors," Appl. Phys. Lett. **81**, 2683–2685 (2002).
[134] L. Gendron, M. Carras, A. Huynh, V. Ortiz, C. Koeniguer, and V. Berger, "Quantum cascade photodetector," Appl. Phys. Lett. **85**, 2824–2826 (2004).
[135] D. Hofstetter, M. Graf, T. Aellen, J. Faist, L. Hvozdara, and S. Blaser, "23 GHz operation of a room temperature photovoltaic quantum cascade detector at 5.35 μm," Appl. Phys. Lett. **89**, 061119 (2006).
[136] F. R. Giorgetta, E. Baumann, R. Théron, M. Pellaton, D. Hofstetter, M. Fischer, and J. Faist, "Short wavelength (4 μm) quantum cascade detector based on strain compensated In Ga As/In Al As," Appl. Phys. Lett. **92**, 121101 (2008).
[137] A. Buffaz, M. Carras, L. Doyennette, A. Nedelcu, X. Marcadet, and V. Berger, "Quantum cascade detectors for very long wave infrared detection," Appl. Phys. Lett. **96**, 172101 (2010).
[138] D. Hofstetter, F. R. Giorgetta, E. Baumann, Q. Yang, C. Manz, and K. Köhler, "Midinfrared quantum cascade detector with a spectrally broad response," Appl. Phys. Lett. **93**, 221106 (2008).
[139] G. Marschick, M. David, E. Arigliani, N. Opačak, B. Schwarz, M. Giparakis, A. Delga, M. Lagree, T. Poletti, V. Trinite *et al.*, "High-responsivity operation of quantum cascade detectors at 9 μm," Opt. Express **30**, 40188–40195 (2022).
[140] B. Schwarz, P. Reininger, A. Harrer, D. MacFarland, H. Detz, A. M. Andrews, W. Schrenk, and G. Strasser, "The limit of quantum cascade detectors: A single period device," Appl. Phys. Lett. **111**, 061107 (2017).
[141] G. Quinchard, C. Mismer, M. Hakl, J. Pereira, Q. Lin, S. Lepillet, V. Trinité, A. Evirgen, E. Peytavit, J. Reverchon *et al.*, "High speed, antenna-enhanced 10.3 μm quantum cascade detector," Appl. Phys. Lett. **120**, 091108 (2022).
[142] B. Schwarz, P. Reininger, H. Detz, T. Zederbauer, A. Maxwell Andrews, S. Kalchmair, W. Schrenk, O. Baumgartner, H. Kosina, and G. Strasser, "A bi-functional quantum cascade device for same-frequency lasing and detection," Appl. Phys. Lett. **101**, 191109 (2012).
[143] A. Spott, J. Peters, M. L. Davenport, E. J. Stanton, C. D. Merritt, W. W. Bewley, I. Vurgaftman, C. S. Kim, J. R. Meyer, J. Kirch *et al.*, "Quantum cascade laser on silicon," Optica **3**, 545–551 (2016).
[144] A. Vardi, N. Kheirodin, L. Nevou, H. Machhadani, L. Vivien, P. Crozat, M. Tchernycheva, R. Colombelli, F. Julien, F. Guillot *et al.*, "High-speed operation of GaN/AlGaN quantum cascade detectors at $\lambda \approx 1.55$ μm," Appl. Phys. Lett. **93**, 193509 (2008).
[145] A. Delga, "Quantum cascade detectors: A review," in *Mid-Infrared Optoelectronics*, *Woodhead Publishing Series in Electronic and Optical Materials*, edited by E. Tournié and L. Cerutti (Woodhead Publishing, 2020), Chap. 8, pp. 337–377.
[146] J. V. Li, R. Q. Yang, C. J. Hill, and S. L. Chuang, "Interband cascade detectors with room temperature photovoltaic operation," Appl. Phys. Lett. **86**, 101102 (2005).
[147] R. Q. Yang, Z. Tian, Z. Cai, J. Klem, M. B. Johnson, and H. Liu, "Interband-cascade infrared photodetectors with superlattice absorbers," J. Appl. Phys. **107**, 054514 (2010).
[148] R. T. Hinkey and R. Q. Yang, "Theory of multiple-stage interband photovoltaic devices and ultimate performance limit comparison of multiple-stage and single-stage interband infrared detectors," J. Appl. Phys. **114**, 104506 (2013).
[149] W. Huang, L. Li, L. Lei, J. A. Massengale, R. Q. Yang, T. D. Mishima, and M. B. Santos, "Electrical gain in interband cascade infrared photodetectors," J. Appl. Phys. **123**, 113104 (2018).
[150] A. Rogalski, P. Martyniuk, and M. Kopytko, "InAs/GaSb type-II superlattice infrared detectors: Future prospect," Appl. Phys. Rev. **4**, 031304 (2017).
[151] W. Huang, S. S. Rassel, L. Li, J. A. Massengale, R. Q. Yang, T. D. Mishima, and M. B. Santos, "A unified figure of merit for interband and intersubband cascade devices," Infrared Phys. Technol. **96**, 298–302 (2019).
[152] Z. Xie, J. Huang, X. Chai, Z. Deng, Y. Chen, Q. Lu, Z. Xu, J. Chen, Y. Zhou, and B. Chen, "High-speed mid-wave infrared interband cascade photodetector at room temperature," Opt. Express **28**, 36915–36923 (2020).

[153] L. Lei, L. Li, H. Lotfi, H. Ye, R. Q. Yang, T. D. Mishima, M. B. Santos, and M. B. Johnson, "Midwavelength interband cascade infrared photodetectors with superlattice absorbers and gain," Opt. Eng. **57**, 011006 (2017).
[154] L. M. Krüger, J. Hillbrand, J. Heidrich, M. Beiser, R. Weih, J. Koeth, C. R. Phillips, B. Schwarz, G. Strasser, and U. Keller, "High-speed interband cascade infrared photodetectors: Photo-response saturation by a femtosecond oscillator," Opt. Express **29**, 14087–14100 (2021).
[155] P. Didier, H. Knötig, O. Spitz, L. Cerutti, A. Lardschneider, E. Awwad, D. Diaz-Thomas, A. N. Baranov, R. Weih, J. Koeth, B. Schwarz, and F. Grillot, "Interband cascade technology for energy-efficient mid-infrared free-space communication," Photonics Res. **11**, 582–590 (2023).
[156] J. Huang, Z. Xie, Y. Chen, J. E. Bowers, and B. Chen, "High speed mid-wave infrared uni-traveling carrier photodetector," IEEE J. Quantum Electron. **56**, 1–7 (2020).
[157] E. A. DeCuir, Jr., G. P. Meissner, P. S. Wijewarnasuriya, N. Gautam, S. Krishna, N. K. Dhar, R. E. Welser, and A. K. Sood, "Long-wave type-II superlattice detectors with unipolar electron and hole barriers," Opt. Eng. **51**, 124001 (2012).
[158] E. Plis, J.-B. Rodriguez, G. Balakrishnan, Y. Sharma, H. Kim, T. Rotter, and S. Krishna, "Mid-infrared InAs/GaSb strained layer superlattice detectors with nBn design grown on a GaAs substrate," Semicond. Sci. Technol. **25**, 085010 (2010).
[159] K. Huang, Y. Wang, J. Fang, W. Kang, Y. Sun, Y. Liang, Q. Hao, M. Yan, and H. Zeng, "Mid-infrared photon counting and resolving via efficient frequency upconversion," Photonics Res. **9**, 259–265 (2021).
[160] J. Huang, Z. Shen, Z. Wang, Z. Zhou, Z. Wang, B. Peng, W. Liu, Y. Chen, and B. Chen, "High-speed mid-wave infrared uni-traveling carrier photodetector based on InAs/InAsSb type-II superlattice," IEEE Electron Device Lett. **43**, 745–748 (2022).
[161] R. Marsland, S. Jacobs, C. L. Canedy, C. Ellis, C. S. Kim, E. M. Jackson, I. Vurgaftman, B. Kolasa, V. Jayaraman, M. Turville-Heitz, T. Earles, S. Ruder, B. Knipfer, J. H. Ryu, J. R. Meyer, D. Botez, and L. J. Mawst, "Multi-Gb/s free-space laser communication at 4.6-μm wavelength using a high-speed, room-temperature, resonant-cavity infrared detector (RCID) and a quantum-cascade laser," Opt. Express **32**, 22479–22492 (2024).
[162] A. Soibel, M. W. Wright, W. H. Farr, S. A. Keo, C. J. Hill, R. Q. Yang, and H. C. Liu, "Midinfrared interband cascade laser for free space optical communication," IEEE Photonics Technol. Lett. **22**, 121–123 (2010).
[163] H. Kim, P. Didier, S. Zaminga, D. Díaz-Thomas, A. Baranov, J. Rodriguez, E. Tournié, H. Knötig, B. Schwarz, L. Cerutti, O. Spitz, and F. Grillot, "Intensity noise and modulation dynamics of an epitaxial mid-infrared interband cascade laser on silicon," APL Photonics **9**, 106103 (2024).
[164] F. Goodwin, "8.4 - A 3.39-micron infrared optical heterodyne communication system," IEEE J. Quantum Electron. **3**, 524–531 (1967).
[165] F. Goodwin and T. Nussmeier, "Optical heterodyne communications experiments at 10.6 μ," IEEE J. Quantum Electron. **4**, 612–617 (1968).
[166] H. W. Mocker, "A 10.6-μ optical heterodyne communication system," Appl. Opt. **8**, 677–684 (1969).
[167] J. H. McElroy, N. McAvoy, E. H. Johnson, J. J. Degnan, F. E. Goodwin, D. M. Henderson, T. A. Nussmeier, L. S. Stokes, B. J. Peyton, and T. Flattau, "CO_2 laser communication systems for near-earth space applications," Proc. IEEE **65**, 221–251 (1977).
[168] R. Martini, R. Paiella, C. Gmachl, F. Capasso, E. Whittaker, H. Liu, H. Hwang, D. Sivco, J. Baillargeon, and A. Cho, "High-speed digital data transmission using mid-infrared quantum cascade lasers," Electron. Lett. **37**, 1290–1292 (2001).
[169] R. Martini and E. A. Whittaker, "Quantum cascade laser-based free space optical communications," J. Opt. Fiber Commun. Rep. **2**, 279–292 (2005).
[170] S. Blaser, D. Hofstetter, M. Beck, and J. Faist, "Free-space optical data link using Peltier-cooled quantum cascade laser," Electron. Lett. **37**, 778–780 (2001).
[171] J. J. Liu, B. L. Stann, K. K. Klett, P. S. Cho, and P. M. Pellegrino, "Mid and long-wave infrared free-space optical communication," Proc. SPIE **11133**, 1113302 (2019).
[172] M. Joharifar, H. Dely, X. Pang, R. Schatz, D. Gacemi, T. Salgals, A. Udalcovs, Y.-T. Sun, Y. Fan, L. Zhang, E. Rodriguez, S. Spolitis, V. Bobrovs, X. Yu, S. Lourdudoss, S. Popov, A. Vasanelli, O. Ozolins, and C. Sirtori, "High-speed 9.6-μm long-wave infrared free-space transmission with a directly-modulated QCL and a fully-passive QCD," J. Lightwave Technol. **41**, 1087–1094 (2023).
[173] M. Joharifar, L. Durupt, H. Dely, A. Ostrovskis, R. Schatz, R. Puerta, G. Maisons, T. Salgals, D. Gacemi, L. Zhang, S. Spolitis, Y.-T. Sun, V. Bobrovs, X. Yu, A. Vasanelli, O. Ozolins, C. Sirtori, and X. Pang, "Advancing LWIR FSO communication through high-speed multilevel signals and directly modulated quantum cascade lasers," Opt. Express **32**, 29138 (2024).
[174] X. Pang, R. Schatz, M. Joharifar, H. Dely, L. Durupt, G. Maisons, D. Gacemi, R. Puerta, T. Bonazzi, L. Zhang, S. Spolitis, Y.-T. Sun, V. Bobrovs, X. Yu, A. Vasanelli, C. Sirtori, and O. Ozolins, "Free space communication enabled by directly modulated quantum cascade laser," in *2024 Optical Fiber Communication Conference (OFC)* (IEEE, Washington, DC, 2024).
[175] H. Dely, M. Joharifar, L. Durupt, A. Ostrovskis, R. Schatz, T. Bonazzi, G. Maisons, D. Gacemi, T. Salgals, L. Zhang, S. Spolitis, Y.-T. Sun, V. Bobrovs, X. Yu, I. Sagnes, K. Pantzas, A. Vasanelli, O. Ozolins, X. Pang, and C. Sirtori, "Unipolar quantum optoelectronics for high speed direct modulation and transmission in 8–14 μm atmospheric window," Nat. Commun. **15**, 8040 (2024).
[176] H. Dely, T. Bonazzi, O. Spitz, E. Rodriguez, D. Gacemi, Y. Todorov, K. Pantzas, G. Beaudoin, I. Sagnes, L. Li *et al.*, "10 Gbit s^{-1} free space data transmission at 9 μm wavelength with unipolar quantum optoelectronics," Laser Photonics Rev. **16**, 2100414 (2022).
[177] T. Bonazzi, H. Dely, P. Didier, D. Gacemi, B. Fix, M. Beck, J. Faist, A. Harouri, I. Sagnes, F. Grillot, A. Vasanelli, and C. Sirtori, "Metamaterial unipolar quantum optoelectronics for mid-infrared free-space optics," APL Photonics **9**, 110801 (2024).
[178] D. Zheng, L. A. Gordon, Y. S. Wu, R. S. Feigelson, M. M. Fejer, R. L. Byer, and K. L. Vodopyanov, "16-μm infrared generation by difference-frequency mixing in diffusion-bonded-stacked GaAs," Opt. Lett. **23**, 1010–1012 (1998).
[179] R. Demur, A. Grisard, L. Morvan, E. Lallier, N. Treps, and C. Fabre, "High sensitivity narrowband wavelength mid-infrared detection at room temperature," Opt. Lett. **42**, 2006–2009 (2017).
[180] A. C. Gray, S. A. Berry, L. G. Carpenter, J. C. Gates, C. B. E. Gawith, and P. G. R. Smith, "Upconversion detection of 1.25 Gb/s mid-infrared telecommunications using a silicon avalanche photodiode," Opt. Express **28**, 34279–34289 (2020).
[181] R. A. Battle, A. M. Chandran, T. H. Runcorn, A. Mussot, A. Kudlinski, R. T. Murray, and J. Roy Taylor, "Mid-infrared difference-frequency generation directly pumped by a fiber four-wave mixing source," Opt. Lett. **48**, 387–390 (2023).
[182] L. Guo, L. Wang, Q. Sun, M. Liu, G. Wang, W. Wang, P. Xie, W. Fan, and W. Zhao, "Mid-infrared dual-comb generation via the cross-phase modulation effect in a normal-dispersion microcavity," Appl. Opt. **59**, 2101–2107 (2020).
[183] Y. Peng, W. Wang, X. Wei, and D. Li, "High-efficiency mid-infrared optical parametric oscillator based on PPMgO:CLN," Opt. Lett. **34**, 2897–2899 (2009).
[184] Y. Matsui, R. Schatz, D. Che, F. Khan, M. Kwakernaak, and T. Sudo, "Low-chirp isolator-free 65-GHz-bandwidth directly modulated lasers," Nat. Photonics **15**, 59–63 (2021).
[185] L. A. Coldren, S. W. Corzine, and M. L. Mashanovitch, *Diode Lasers and Photonic Integrated Circuits* (John Wiley & Sons, 2012).
[186] P. S. Cho, G. Harston, K.-D. F. Büchter, D. Soreide, J. M. Saint Clair, W. Sohler, Y. Achiam, and I. Shpantzer,"Optical homodyne RZ-QPSK transmission through wind tunnel at 3.8 and 1.55 μm via wavelength conversion," Proc. SPIE **7324**, 73240A (2009).
[187] K. Zou, K. Pang, H. Song, J. Fan, Z. Zhao, H. Song, R. Zhang, H. Zhou, A. Minoofar, C. Liu, X. Su, N. Hu, A. McClung, M. Torfeh, A. Arbabi, M. Tur, and A. E. Willner, "High-capacity free-space optical communications using wavelength- and mode-division-multiplexing in the mid-infrared region," Nat. Commun. **13**, 7662 (2022).
[188] H. Zhou, Y. Duan, M. Ramakrishnan, Z. Jiang, X. Su, K. Zou, A. T. Heiniger, M. Tur, and A. E. Willner, "Demonstration of an optical parametric oscillator (OPO)-based high-power data transmitter for a 10-Gbit/s QPSK mid-IR coherent free-space link through fog," J. Lightwave Technol. **42**, 3989–3996 (2024).
[189] A. Grisard, E. Lallier, and B. Gérard, "Quasi-phase-matched gallium arsenide for versatile mid-infrared frequency conversion," Opt. Mater. Express **2**, 1020–1025 (2012).
[190] T. H. Stievater, R. Mahon, D. Park, W. S. Rabinovich, M. W. Pruessner, J. B. Khurgin, and C. J. K. Richardson, "Mid-infrared difference-frequency generation in suspended GaAs waveguides," Opt. Lett. **39**, 945–948 (2014).

[191] J. Wueppen, S. Nyga, B. Jungbluth, and D. Hoffmann, "1.95 μm-pumped OP-GaAs optical parametric oscillator with 10.6 μm idler wavelength," Opt. Lett. **41**, 4225–4228 (2016).

[192] V. L. Tassev, S. R. Vangala, R. D. Peterson, M. M. Kimani, M. Snure, R. W. Stites, S. Guha, J. E. Slagle, T. R. Ensley, A. A. Syed, and I. V. Markov, "Heteroepitaxial growth of OPGaP on OPGaAs for frequency conversion in the IR and THz," Opt. Mater. Express **6**, 1724–1737 (2016).

[193] G. Insero, C. Clivati, D. D'Ambrosio, P. D. Natale, G. Santambrogio, P. G. Schunemann, J.-J. Zondy, and S. Borri, "Difference frequency generation in the mid-infrared with orientation-patterned gallium phosphide crystals," Opt. Lett. **41**, 5114–5117 (2016).

[194] J. Wei, S. C. Kumar, H. Ye, P. G. Schunemann, and M. Ebrahim-Zadeh, "Performance characterization of mid-infrared difference-frequency-generation in orientation-patterned gallium phosphide," Opt. Mater. Express **8**, 555–567 (2018).

[195] Y. Su, J. Meng, T. Wei, Z. Xie, S. Jia, W. Tian, J. Zhu, and W. Wang, "150 Gbps multi-wavelength FSO transmission with 25-GHz ITU-T grid in the mid-infrared region," Opt. Express **31**, 15156–15169 (2023).

[196] L. Gu, Z. Tan, Q. Wu, C. Wang, and J. Cao, "20 Mbps wireless communication demonstration using terahertz quantum devices," Chin. Opt. Lett. **13**, 081402 (2015).

[197] R. Martini, C. Gmachl, J. Falciglia, F. G. Curti, C. G. Bethea, F. Capasso, E. A. Whittaker, R. Paiella, A. Tredicucci, A. L. Hutchinson *et al.*, "High-speed modulation and free-space optical audio/video transmission using quantum cascade lasers," Electron. Lett. **37**, 191–193 (2001).

[198] R. Martini, C. Bethea, F. Capasso, C. Gmachl, R. Paiella, E. Whittaker, H. Hwang, D. Sivco, J. Baillargeon, and A. Cho, "Free-space optical transmission of multimedia satellite data streams using mid-infrared quantum cascade lasers," Electron. Lett. **38**(4), 181–183 (2002).

[199] M. Taslakov, V. Simeonov, and H. van den Bergh, "Line-of-sight data transmission system based on mid IR quantum cascade laser," Proc. SPIE **6877**, 68770F (2008).

[200] E. Ip, D. Buchter, C. Langrock, J. M. Kahn, H. Herrmann, W. Sohler, and M. M. Fejer, "QPSK transmission over free-space link at 3.8 μm using coherent detection with wavelength conversion," in *2008 34th European Conference on Optical Communication* (IEEE, 2008), pp. 1–2.

[201] C. Liu, S. Zhai, J. Zhang, Y. Zhou, Z. Jia, F. Liu, and Z. Wang, "Free-space communication based on quantum cascade laser," J. Semicond. **36**, 094009 (2015).

[202] Q. Hao, G. Zhu, S. Yang, K. Yang, T. Duan, X. Xie, K. Huang, and H. Zeng, "Mid-infrared transmitter and receiver modules for free-space optical communication," Appl. Opt. **56**, 2260–2264 (2017).

[203] X. Pang, O. Ozolins, R. Schatz, J. Storck, A. Udalcovs, J. R. Navarro, A. Kakkar, G. Maisons, M. Carras, G. Jacobsen, S. Popov, and S. Lourdudoss, "Gigabit free-space multi-level signal transmission with a mid-infrared quantum cascade laser operating at room temperature," Opt. Lett. **42**, 3646–3649 (2017).

[204] X. Pang, O. Ozolins, L. Zhang, R. Schatz, A. Udalcovs, J. Storck, G. Maisons, M. Carras, S. Xiao, G. Jacobsen, S. Popov, J. Chen, and S. Lourdudoss, "4 Gbps PAM-4 and DMT free space transmission using a 4.65-pm quantum cascaded laser at room temperature," in *2017 European Conference on Optical Communication (ECOC)* (IEEE, 2017), pp. 1–3.

[205] Y. Su, W. Wang, X. Hu, H. Hu, X. Huang, Y. Wang, J. Si, X. Xie, B. Han, H. Feng, Q. Hao, G. Zhu, T. Duan, and W. Zhao, "10 Gbps DPSK transmission over free-space link in the mid-infrared," Opt. Express **26**, 34515 (2018).

[206] W. Wang, Y. Zheng, X. Xie, Y. Su, X. Huang, T. Duan, and W. Zhao, "5 Gbaud QPSK coherent transmission in the mid-infrared," Opt. Commun. **466**, 125681 (2020).

[207] O. Spitz, P. Didier, L. Durupt, D. A. Díaz-Thomas, A. N. Baranov, L. Cerutti, and F. Grillot, "Free-space communication with directly modulated mid-infrared quantum cascade devices," IEEE J. Sel. Top. Quantum Electron. **28**, 1200109 (2022).

[208] X. Pang, R. Schatz, M. Joharifar, A. Udalcovs, V. Bobrovs, L. Zhang, X. Yu, Y. T. Sun, G. Maisons, M. Carras, S. Popov, S. Lourdudoss, and O. Ozolins, "Direct modulation and free-space transmissions of up to 6 Gbps multilevel signals with a 4.65-μQuantum cascade laser at room temperature," J. Lightwave Technol. **40**, 2370–2377 (2022).

[209] O. Spitz, K. Yang, A. Guillaume-Manca, P. Didier, J. Liu, and F. Grillot, "Multi-Gb/s free-space communication with energy-efficient room-temperature quantum cascade laser emitting at 8.1 μm," in *2021 IEEE Photonics Conference (IPC)* (IEEE, 2021), pp. 1–2.

[210] N. Corrias, T. Gabbrielli, P. De Natale, L. Consolino, and F. Cappelli, "Analog FM free-space optical communication based on a mid-infrared quantum cascade laser frequency comb," Opt. Express **30**, 10217–10228 (2022).

[211] H. Dely, M. Joharifar, X. Pang, D. Gacemi, T. Salgals, R. Schatz, Y.-T. Sun, T. Bonazzi, E. Rodriguez, Y. Todorov, A. Vasanelli, A. Udalcovs, S. Spolitis, V. Bobrovs, O. Ozolins, S. Popov, and C. Sirtori, "High bitrate data transmission in the 8-14 μm atmospheric window using an external Stark-effect modulator with digital equalization," Opt. Express **31**, 7259–7264 (2023).

[212] M. Han, M. Joharifar, M. Wang, Y. Fan, G. Maisons, J. Abautret, Y.-T. Sun, R. Teissier, L. Zhang, V. Bobrovs, X. Yu, R. Schatz, S. Popov, O. Ozolins, and X. Pang, "Long-wave infrared discrete multitone free-space transmission using a 9.15-μm quantum cascade laser," IEEE Photonics Technol. Lett. **35**, 489–492 (2023).

[213] M. Han, M. Joharifar, M. Wang, R. Schatz, R. Puerta, Y.-t. Sun, Y. Fan, G. Maisons, J. Abautret, R. Teissier, L. Zhang, S. Spolitis, V. Bobrovs, S. Lourdudoss, X. Yu, S. Popov, O. Ozolins, and X. Pang, "High spectral efficiency long-wave infrared free-space optical transmission with multilevel signals," J. Lightwave Technol. **41**, 6514–6520 (2023).

[214] M. Joharifar, M. Han, R. Schatz, R. Puerta, Y.-T. Sun, Y. Fan, G. Maisons, J. Abautret, R. Teissier, L. Zhang, S. Spolitis, M. Wang, V. Bobrovs, S. Lourdudoss, X. Yu, S. Popov, O. Ozolins, and X. Pang, "8.1 Gbps PAM8 long-wave IR FSO transmission using a 9.15-μm directly-modulated QCL with an MCT detector," in *2023 Optical Fiber Communication Conference (OFC)* (IEEE, 2023), p. Th1H.1.

[215] Y. Su, W. Tian, Y. Yu, J. Meng, Y. Zheng, S. Jia, Z. Xie, Y. Wang, J. Zhu, and W. Wang, "Free-space transmission of picosecond-level, high-speed optical pulse streams in the 3 μm band," Opt. Express **31**, 27433–27449 (2023).

[216] J. Ohtsubo, *Semiconductor Lasers: Stability, Instability and Chaos* (Springer, 2012), Vol. 111.

[217] A. Argyris, D. Syvridis, L. Larger, V. Annovazzi-Lodi, P. Colet, I. Fischer, J. Garcia-Ojalvo, C. R. Mirasso, L. Pesquera, and K. A. Shore, "Chaos-based communications at high bit rates using commercial fibre-optic links," Nature **438**, 343–346 (2005).

[218] Y. Xie, Z. Yang, M. Shi, Q. Zhuge, W. Hu, and L. Yi, "100 Gb/s coherent chaotic optical communication over 800 km fiber transmission via advanced digital signal processing," Adv. Photonics **3**, 016003 (2024).

[219] O. Spitz, A. Herdt, J. Wu, G. Maisons, M. Carras, C.-W. Wong, W. Elsäßer, and F. Grillot, "Private communication with quantum cascade laser photonic chaos," Nat. Commun. **12**, 3327 (2021).

[220] P. Didier, S. Zaminga, O. Spitz, J. Wu, E. Awwad, G. Maisons, and F. Grillot, "Data encryption with chaotic light in the long wavelength infrared atmospheric window," Optica **11**, 626 (2024).

[221] Secure mid-wave free-space mid-wave infrared optical communication using chaotic laser mode, navy STTR 23.B - Topic N23B-T030" (2023).

[222] M. Milanizadeh, S. SeyedinNavadeh, F. Zanetto, V. Grimaldi, C. De Vita, C. Klitis, M. Sorel, G. Ferrari, D. A. B. Miller, A. Melloni, and F. Morichetti, "Separating arbitrary free-space beams with an integrated photonic processor," Light: Sci. Appl. **11**, 197 (2022).

[223] S. SeyedinNavadeh, M. Milanizadeh, F. Zanetto, G. Ferrari, M. Sampietro, M. Sorel, D. A. B. Miller, A. Melloni, and F. Morichetti, "Determining the optimal communication channels of arbitrary optical systems using integrated photonic processors," Nat. Photonics **18**, 149–155 (2024).

[224] H. Nguyen-Van, A. N. Baranov, Z. Loghmari, L. Cerutti, J.-B. Rodriguez, J. Tournet, G. Narcy, G. Boissier, G. Patriarche, M. Bahriz *et al.*, "Quantum cascade lasers grown on silicon," Sci. Rep. **8**, 7206 (2018).

[225] S. Jung, J. Kirch, J. H. Kim, L. J. Mawst, D. Botez, and M. A. Belkin, "Quantum cascade lasers transfer-printed on silicon-on-sapphire," Appl. Phys. Lett. **111**, 211102 (2017).

[226] E. Tournié, L. Monge Bartolome, M. Rio Calvo, Z. Loghmari, D. A. Díaz-Thomas, R. Teissier, A. N. Baranov, L. Cerutti, and J.-B. Rodriguez, "Mid-infrared III–V semiconductor lasers epitaxially grown on Si substrates," Light: Sci. Appl. **11**, 165 (2022).

[227] J. Ramirez, Q. Liu, V. Vakarin, J. Frigerio, A. Ballabio, X. Le Roux, D. Bouville, L. Vivien, G. Isella, and D. Marris-Morini, "Graded SiGe waveguides with

broadband low-loss propagation in the mid infrared," Opt. Express **26**, 870–877 (2018).

[228] B. Dror, Y. Zheng, M. Agrawal, K. Radhakrishnan, M. Orenstein, and G. Bahir, "Mid-infrared GaN/AlGaN quantum cascade detector grown on silicon," IEEE Electron Device Lett. **40**, 263–266 (2019).

[229] M. Montesinos-Ballester, C. Lafforgue, J. Frigerio, A. Ballabio, V. Vakarin, Q. Liu, J. M. Ramirez, X. Le Roux, D. Bouville, A. Barzaghi *et al.*, "On-chip mid-infrared supercontinuum generation from 3 to 13 μm wavelength," ACS Photonics **7**, 3423–3429 (2020).

[230] A. Spott, E. J. Stanton, N. Volet, J. D. Peters, J. R. Meyer, and J. E. Bowers, "Heterogeneous integration for mid-infrared silicon photonics," IEEE J. Sel. Top. Quantum Electron. **23**, 8200810 (2017).

[231] Y. Zou, S. Chakravarty, C.-J. Chung, X. Xu, and R. T. Chen, "Mid-infrared silicon photonic waveguides and devices [Invited]," Photonics Res. **6**, 254–276 (2018).

[232] S. Jung, D. Palaferri, K. Zhang, F. Xie, Y. Okuno, C. Pinzone, K. Lascola, and M. A. Belkin, "Homogeneous photonic integration of mid-infrared quantum cascade lasers with low-loss passive waveguides on an InP platform," Optica **6**, 1023–1030 (2019).

[233] M. Graf, N. Hoyler, M. Giovannini, J. Faist, and D. Hofstetter, "InP-based quantum cascade detectors in the mid-infrared," Appl. Phys. Lett. **88**, 241118 (2006).

[234] C. Gilles, L. J. Orbe, G. Carpintero, J. Abautret, G. Maisons, and M. Carras, "Monolithic integration of a quantum cascade laser array and an echelle grating multiplexer for widely tunable mid-infrared sources," Proc. SPIE **9767**, 97671R (2016).

[235] K. M. Yoo, J. Midkiff, A. Rostamian, C.-j. Chung, H. Dalir, and R. T. Chen, "InGaAs membrane waveguide: A promising platform for monolithic integrated mid-infrared optical gas sensor," ACS Sens. **5**, 861–869 (2020).

[236] T. S. Karnik, K. P. Dao, Q. Du, L. Diehl, C. Pflügl, D. Vakhshoori, and J. Hu, "High-efficiency mid-infrared InGaAs/InP arrayed waveguide gratings," Opt. Express **31**, 5056–5068 (2023).

[237] K. Zhang, D. Burghart, E. De Toma, R. Mayer, A. Gardanow, G. Boehm, and M. Belkin, "Mid-infrared photonic integration on InP," Proc. SPIE **PC12440**, PC124400K (2023).

[238] D. Burghart, K. Zhang, G. Boehm, and M. Belkin, "Multiplexed quantum cascade laser sources for multi-species gas sensing using photonic integration," Proc. SPIE **PC12440**, PC124400T (2023).

[239] D. Kazakov, T. P. Letsou, M. Beiser, Y. Zhi, N. Opačak, M. Piccardo, B. Schwarz, and F. Capasso, "Active mid-infrared ring resonators," Nat. Commun. **15**, 607 (2024).

[240] K. Zhang, G. Böhm, and M. A. Belkin, "Mid-infrared microring resonators and optical waveguides on an InP platform," Appl. Phys. Lett. **120**, 061106 (2022).

[241] M. Montesinos-Ballester, E. Jöchl, V. Turpaud, J. Hillbrand, M. Bertrand, D. Marris-Morini, E. Gini, and J. Faist, "Low-loss buried InGaAs/InP integrated waveguides in the long-wave infrared," ACS Photonics **11**, 2236–2241 (2024).

[242] B. Schwarz, C. A. Wang, L. Missaggia, T. S. Mansuripur, P. Chevalier, M. K. Connors, D. McNulty, J. Cederberg, G. Strasser, and F. Capasso, "Watt-level continuous-wave emission from a bifunctional quantum cascade laser/detector," ACS Photonics **4**, 1225–1231 (2017).

[243] B. Schwarz, P. Reininger, D. Ristanić, H. Detz, A. M. Andrews, W. Schrenk, and G. Strasser, "Monolithically integrated mid-infrared lab-on-a-chip using plasmonics and quantum cascade structures," Nat. Commun. **5**, 4085 (2014).

[244] M. David, A. Dabrowska, M. Sistani, I. C. Doganlar, E. Hinkelmann, H. Detz, W. M. Weber, B. Lendl, G. Strasser, and B. Hinkov, "Octave-spanning low-loss mid-IR waveguides based on semiconductor-loaded plasmonics," Opt. Express **29**, 43567–43579 (2021).

[245] M. David, D. Disnan, E. Arigliani, A. Lardschneider, G. Marschick, H. T. Hoang, H. Detz, B. Lendl, U. Schmid, G. Strasser, and B. Hinkov, "Advanced mid-infrared plasmonic waveguides for on-chip integrated photonics," Photonics Res. **11**, 1694–1702 (2023).

[246] R. Wang, P. Täschler, Z. Wang, E. Gini, M. Beck, and J. Faist, "Monolithic integration of mid-infrared quantum cascade lasers and frequency combs with passive waveguides," ACS Photonics **9**, 426–431 (2022).

[247] W. Zhou, D. Wu, Q.-Y. Lu, S. Slivken, and M. Razeghi, "Single-mode, high-power, mid-infrared, quantum cascade laser phased arrays," Sci. Rep. **8**, 14866 (2018).

[248] T. S. Karnik, L. Diehl, K. P. Dao, Q. Du, C. Pflügl, D. Vakhshoori, and J. Hu, "Monolithic beam combined quantum cascade laser arrays with integrated arrayed waveguide gratings," Opt. Express **32**, 11681–11692 (2024).

[249] C. Gilles, L. J. Orbe, G. Carpintero, G. Maisons, and M. Carras, "Mid-infrared wavelength multiplexer in InGaAs/InP waveguides using a Rowland circle grating," Opt. Express **23**, 20288–20296 (2015).

[250] J. Hillbrand, A. M. Andrews, H. Detz, G. Strasser, and B. Schwarz, "Coherent injection locking of quantum cascade laser frequency combs," Nat. Photonics **13**, 101–104 (2019); arXiv:1808.06636.

[251] A. Delga and L. Leviandier, "Free-space optical communications with quantum cascade lasers," Proc. SPIE **10926**, 1092617 (2019).

[252] A. G. Davies, A. D. Burnett, W. Fan, E. H. Linfield, and J. E. Cunningham, "Terahertz spectroscopy of explosives and drugs," Mater. Today **11**, 18–26 (2008).

[253] M. I. Amanti, G. Scalari, M. Beck, and J. Faist, "Stand-alone system for high-resolution, real-time terahertz imaging," Opt. Express **20**, 2772–2778 (2012).

[254] J. Federici and L. Moeller, "Review of terahertz and subterahertz wireless communications," J. Appl. Phys. **107**, 111101 (2010).

[255] A. Rogalski and F. Sizov, "Terahertz detectors and focal plane arrays," Opto-Electron. Rev. **19**, 346–404 (2011).

[256] K. Balakier, M. J. Fice, F. van Dijk, G. Kervella, G. Carpintero, A. J. Seeds, and C. C. Renaud, "Optical injection locking of monolithically integrated photonic source for generation of high purity signals above 100 GHz," Opt. Express **22**, 29404–29412 (2014).

[257] X. Pang, A. Caballero, A. Dogadaev, V. Arlunno, R. Borkowski, J. S. Pedersen, L. Deng, F. Karinou, F. Roubeau, D. Zibar *et al.*, "100 Gbit/s hybrid optical fiber-wireless link in the W-band (75–110 GHz)," Opt. Express **19**, 24944–24949 (2011).

[258] G. Ducournau, K. Engenhardt, P. Szriftgiser, D. Bacquet, M. Zaknoune, R. Kassi, E. Lecomte, and J.-F. Lampin, "32 Gbit/s QPSK transmission at 385 GHz using coherent fibre-optic technologies and THz double heterodyne detection," Electron. Lett. **51**, 915–917 (2015).

[259] S. Jia, M.-C. Lo, L. Zhang, O. Ozolins, A. Udalcovs, D. Kong, X. Pang, R. Guzman, X. Yu, S. Xiao *et al.*, "Integrated dual-laser photonic chip for high-purity carrier generation enabling ultrafast terahertz wireless communications," Nat. Commun. **13**, 1388 (2022).

[260] A. Calvar, M. I. Amanti, M. Renaudat St-Jean, S. Barbieri, A. Bismuto, E. Gini, M. Beck, J. Faist, and C. Sirtori, "High frequency modulation of mid-infrared quantum cascade lasers embedded into microstrip line," Appl. Phys. Lett. **102**, 181114 (2013).

[261] A. Mottaghizadeh, Z. Asghari, M. Amanti, D. Gacemi, A. Vasanelli, and C. Sirtori, "Ultra-fast modulation of mid infrared buried heterostructure quantum cascade lasers," in *2017 42nd International Conference on Infrared, Millimeter, and Terahertz Waves (IRMMW-THz)* (IEEE, 2017), pp. 1–2.

[262] P. Grant, R. Dudek, M. Buchanan, and H. Liu, "Room-temperature heterodyne detection up to 110 GHz with a quantum-well infrared photodetector," IEEE Photonics Technol. Lett. **18**, 2218–2220 (2006).

[263] B. Meng and Q. J. Wang, "Theoretical investigation of injection-locked high modulation bandwidth quantum cascade lasers," Opt. Express **20**, 1450–1464 (2012).

[264] C. Wang, F. Grillot, V. Kovanis, and J. Even, "Rate equation analysis of injection-locked quantum cascade lasers," J. Appl. Phys. **113**, 063104 (2013).

[265] C. Wang, F. Grillot, V. I. Kovanis, J. D. Bodyfelt, and J. Even, "Modulation properties of optically injection-locked quantum cascade lasers," Opt. Lett. **38**, 1975–1977 (2013).

[266] R. Paiella, R. Martini, F. Capasso, C. Gmachl, H. Y. Hwang, D. L. Sivco, J. N. Baillargeon, A. Y. Cho, E. A. Whittaker, and H. Liu, "High-frequency modulation without the relaxation oscillation resonance in quantum cascade lasers," Appl. Phys. Lett. **79**, 2526–2528 (2001).

[267] F. Grillot, P. Didier, O. Spitz, L. D. Balzo, H. Kim, H. Dely, T. Bonazzi, E. Rodriguez, D. Gacemi, A. Vasanelli, and C. Sirtori, "Bridging the 100 GHz-10 THz

domain with unipolar quantum optoelectronics," Proc. SPIE **12230**, 122300A (2022).
[268] M. Troccoli, C. Gmachl, F. Capasso, D. L. Sivco, and A. Y. Cho, "Mid-infrared ($\lambda \approx 7.4$ μm) quantum cascade laser amplifier for high power single-mode emission and improved beam quality," Appl. Phys. Lett. **80**, 4103–4105 (2002).
[269] P. Friedli, H. Sigg, B. Hinkov, A. Hugi, S. Riedi, M. Beck, and J. Faist, "Four-wave mixing in a quantum cascade laser amplifier," Appl. Phys. Lett. **102**, 22104 (2013).
[270] Q. Lu, S. Slivken, D. Wu, and M. Razeghi, "High power continuous wave operation of single mode quantum cascade lasers up to 5 W spanning $\lambda \sim 3.8$-8.3 μm," Opt. Express **28**, 15181–15188 (2020).
[271] Z. Wang, B. Zhang, J. Liu, Y. Song, and H. Zhang, "Recent developments in mid-infrared fiber lasers: Status and challenges," Opt Laser. Technol. **132**, 106497 (2020).
[272] S. D. Jackson, "Mid-infrared fiber laser research: Tasks completed and the tasks ahead," APL Photonics **9**, 070904 (2024).